Acta Mech 228, 2691–2711 (2017)
DOI 10.1007/s00707-017-1846-z

ORIGINAL PAPER

M. Shojaee · A. R. Setoodeh · P. Malekzadeh

Vibration of functionally graded CNTs-reinforced skewed cylindrical panels using a transformed differential quadrature method

Received: 17 September 2016 / Revised: 4 February 2017 / Published online: 6 May 2017

Abstract As a first endeavor, the free vibration behavior of functionally graded carbon nanotubes-reinforced composite (FG-CNTRC) skewed cylindrical panels, as a most general geometry of panels in practical applications, is investigated. The first-order shear deformation shell theory is used to model the kinematics of deformations, and Hamilton's principle is applied to drive the differential governing equations and the related boundary conditions. An analytical transformation together with the differential quadrature method, namely transformed differential quadrature method, is employed to discretize the governing equations subjected to general boundary conditions. This method offers superior practicality and applicability in directly discretizing the governing differential equations for an arbitrary physical domain. The correctness of the computational method is investigated through several numerical examples that include FG-CNTRC skew plates, homogeneous skewed cylindrical panels and FG-CNTRC cylindrical panels. Eventually, the effects of geometrical shape parameters like thickness/radius-to-length and aspect ratios, different distributions and volume fractions of CNTs and boundary conditions on the non-dimensional frequency parameters of the FG-CNTRC skewed cylindrical panels are studied.

1 Introduction

Skewed cylindrical composite panels as one of the important structural components have been extensively used in different branches of modern industrials such as aerospace, automobile, marine, submarine and nuclear technologies. On the other hand, the research to improve the material properties of reinforced composite materials has been continued in recent years. In this regard, it has been shown that CNTs have superior material properties over the micro-sized fibers such as glass, Kevlar and carbon fibers [1–3] and have the potential to be used as an alternative replacement for these conventional reinforcements. For the purpose of effective use of these reinforcements to produce the nanocomposites with the desired performances, it has been suggested to use the engineered gradients of them in the preferred direction [4].

As an important feature of the structural elements, their vibration behavior should be studied carefully for a high-quality design and manufacture. In recent years, the free and forced vibrations of the carbon nanotubes

M. Shojaee · A. R. Setoodeh (✉)
Department of Mechanical and Aerospace Engineering, Shiraz University of Technology, Shiraz 71555, Iran
E-mail: setoodeh@sutech.ac.ir; asetood@yahoo.com
Tel.: +98 71 37264102
Fax: +98 71 37264102

P. Malekzadeh
Department of Mechanical Engineering, School of Engineering, Persian Gulf University, Bushehr 7516913798, Iran

reinforced composite (CNTRC) beams, plates and shells have been investigated in-depth by some researchers; see for examples Refs. [5–72]. However, the research works on the CNTRC shell panels (or incomplete shells) concerned with cylindrical and spherical shell panels with regular boundaries and to the best of authors' knowledge, the CNTRC skewed cylindrical panels have not been analyzed yet. In the following, the recent papers relevant to the present work are reviewed.

Sobhani Aragh et al. [59] used the three-dimensional elasticity theory to study the vibrational behavior of the FG-CNTRC cylindrical panels with two opposite edges simply supported. They provided a semi-analytical solution procedure by employing the two-dimensional generalized differential quadrature method (GDQM) together with the trigonometric series solution.

Shen and Xiang [60,63] presented the nonlinear vibration analysis of the FG-CNTRC cylindrical shells without and with elastic support in thermal environments. The equations of motion were derived based on a higher-order shear deformation theory with von Kármán-type of kinematic nonlinearity. They determined the nonlinear frequencies of the FG-CNTRC shells by employing an improved perturbation technique.

Yas et al. [61] investigated the vibrational characteristics of the FG-CNTRC cylindrical panels with simply supported edges based on the three-dimensional elasticity theory. They applied the trigonometric series solution to discretize the in-plane derivatives and the GDQM to discretize the resulting ordinary equations in the panel thickness.

Pourasghar and Kamarian [62] developed a semi-analytical solution to study the three-dimensional free vibration behavior of the simply supported functionally graded multiwalled carbon nanotubes/phenolic nanocomposite cylindrical panels on elastic foundation. They utilized the modified Halpin–Tasi equation to evaluate the Young's modulus of the MWCNT/epoxy composites by the considering an orientation and an exponential shape factor in the corresponding equation.

Zhang et al. [64] investigated the performance of the mesh-free kp-Ritz method for bending and free vibration analyses of the FG-CNTRC cylindrical panels. The first-order shear deformation theory of shells in conjunction with the Eshelby–Mori–Tanaka approach was used to derive the governing equations.

Lei et al. [65,66] investigated the vibrational behavior of the single layer and laminated FG-CNTRC rotating cylindrical panels based on Love's thin shell theory under different boundary conditions. They evaluated the effective material properties by using the extended rule of mixture and applied the element-free kernel particle Ritz method to discretize the governing equations of motion.

Mirzaei and Kiani [67] proposed a Ritz formulation with Chebyshev polynomials as the basis functions to study the free vibration characteristics of FG-CNTRC cylindrical panels. The Donnell shallow shell theory and first shear order deformation shell theory were used to obtain the governing equations.

Tornabene et al. [69] studied the effect of the agglomeration of the reinforcing phase on the natural frequencies of functionally graded carbon nanotube-reinforced laminated composite doubly curved shells. The theoretical model for shell structures was based on the so-called Carrera unified formulation, and the derived governing equations were solved numerically by means of the GDQM.

Thomas and Roy [70] employed Koiter's shell theory in conjunction with the finite element method to analyze the free vibration behavior of the FG-CNTRC doubly curved shell panels. They used an eight-noded shell element, which includes the transverse shear effect according to Mindlin's hypothesis, to analyze the different types of FG-CNTRC shell structures such as spherical, ellipsoidal, doubly curved and cylindrical.

Pouresmaeeli and Fazelzadeh [71] analyzed the free vibration of moderately thick doubly curved FG-CNTRC doubly curved panels such as spherical, cylindrical and hyperbolic paraboloid panels by utilizing Galerkin's method. The governing differential equations were derived using the first-order shear deformation theory of shells.

As revealed from the literature survey and to the best of authors' knowledge, the vibrational behavior of the FG-CNTRC skewed cylindrical panels has not been investigated yet. Therefore, in this paper, this practically important structural problem is analyzed. For this purpose, the governing differential motion equations and the related boundary conditions of the FG-CNTRC skewed cylindrical panels are derived based on the first-order shear deformation theory of shells using Hamilton's principle. Due to complexity of the governing equations and also to investigate the influences of different types of boundary conditions, an approximate analytical or numerical method should be adopted to solve the equations of motion. To accomplish this major task, an analytical transformation in conjunction with the differential quadrature method, namely TDQM, is introduced. Accordingly, the transformed weighting coefficients are obtained and used to discretize the spatial derivatives of the governing differential equations in a systematic and orderly manner. The accuracy, stability and reliability features of the method are shown through different numerical examples. Then, some numerical studies are

conducted to investigate the effects of geometrical and different material parameters on the non-dimensional frequency parameters of the FG-CNTRC skewed cylindrical panels under different boundary conditions.

2 The geometry and material properties of the panels

In Figs. 1 and 2, the geometry of the FG-CNTRC skewed cylindrical panels under consideration is shown. The cylindrical coordinate system with the coordinate variables x, $s(=R\theta)$ and z is used to label the material points of the panel in the un-deformed reference configuration. As shown in these figures, the panel has a thickness

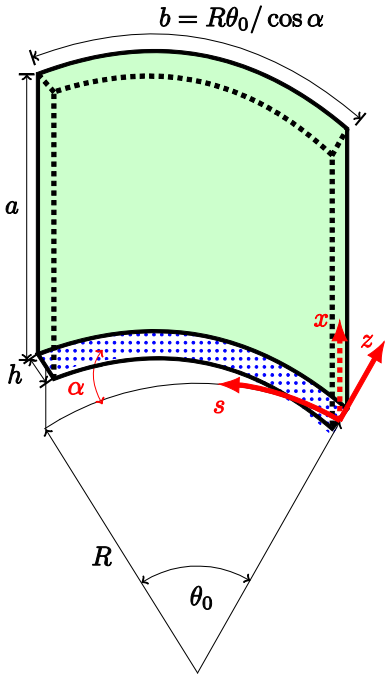

Fig. 1 Geometry of the FG-CNTRC skewed cylindrical panels

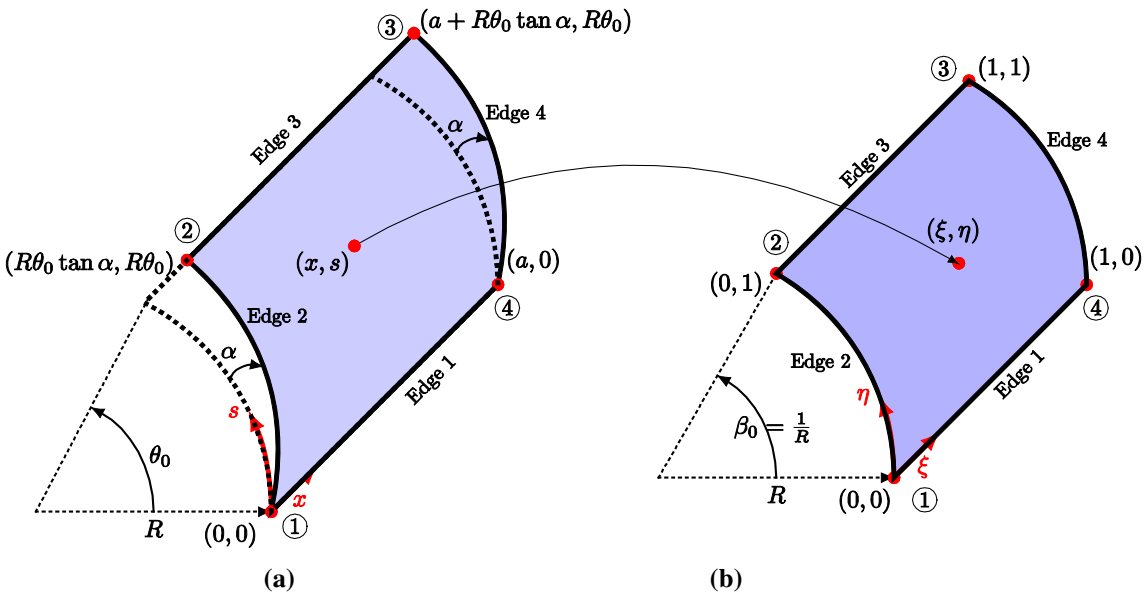

Fig. 2 (**a**, **b**) Geometric transformation, **a** physical domain, **b** computational domain

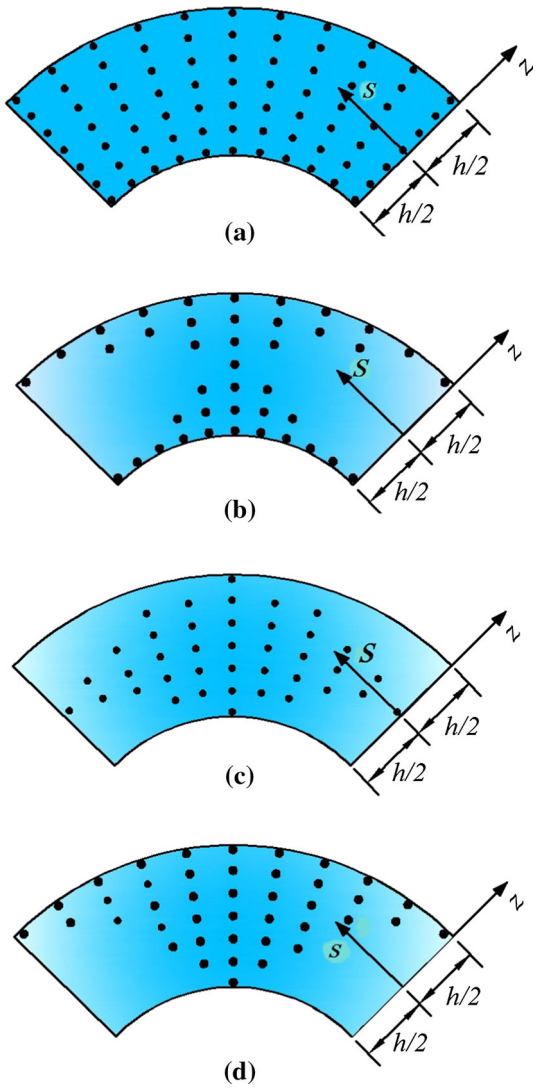

Fig. 3 (**a**)–(**d**) Different arrangement of CNTs distributions through the panel thickness: **a** UD, **b** FG-X, **c** FG-O, **d** FG-V

h, skew angle α, subtended angle θ_0, mean radius R, length a in the x-direction and width b in the oblique direction. The panel is made of a matrix reinforced with straight single-walled carbon nanotubes (SWCNTs) with uniform or non-uniform distribution of CNTs in its thickness direction. The matrix is assumed to be homogeneous and isotropic and has a linear elastic behavior.

Four types of CNTs distribution along the thickness direction are shown in Fig. 3, which are uniformly distributed (UD), FG-X shape, FG-O shape and FG-V shape distributions (see Fig. 3). The corresponding distributions of CNTs along the z-axis are as follows [32]:

$$\text{UD: } V_{\text{CNT}}(z) = V^*_{\text{CNT}} \tag{1a}$$

$$\text{FG-X: } V_{\text{CNT}}(z) = 2\left(\frac{2|z|}{h}\right) V^*_{\text{CNT}} \tag{1b}$$

$$\text{FG-O: } V_{\text{CNT}}(z) = 2\left(1 - \frac{2\,|z|}{h}\right) V^*_{\text{CNT}} \tag{1c}$$

$$\text{FG-V: } V_{\text{CNT}}(z) = \left(1 + \frac{2z}{h}\right) V^*_{\text{CNT}} \tag{1d}$$

where

$$V^*_{\mathrm{CNT}} = \frac{w_{\mathrm{CNT}}}{w_{\mathrm{CNT}} + \left(\frac{\rho^{\mathrm{CNT}}}{\rho^m}\right) - \left(\frac{\rho^{\mathrm{CNT}}}{\rho^m}\right) w_{\mathrm{CNT}}}. \tag{2}$$

In the above equation, w_{CNT} is the mass fraction of nanotubes, and ρ^m and ρ^{CNT} are the densities of matrix and CNTs, respectively. The equivalent Poisson's ratio ν_{12} and density ρ of the panels through the thickness are obtained using general form of the rule of mixture [11,32–36,65–68,70,71]

$$\nu_{12} = V_{\mathrm{CNT}}\nu_{12}^{\mathrm{CNT}} + V_m\nu^m, \quad \rho = V_{\mathrm{CNT}}\rho^{\mathrm{CNT}} + V_m\rho^m. \tag{3a, b}$$

An equivalent continuum model based on the extended rule of mixture approach is employed to estimate the effective Young's modulus (E_{11}, E_{22}) and shear modulus (G_{12}) of FG-CNTRC panels [11,32–36,65–68,70,71]:

$$E_{11} = \eta_1 V_{\mathrm{CNT}} E_{11}^{\mathrm{CNT}} + V_m E^m, \quad \frac{\eta_2}{E_{22}} = \frac{V_{\mathrm{CNT}}}{E_{22}^{\mathrm{CNT}}} + \frac{V_m}{E^m}, \quad \frac{\eta_3}{G_{12}} = \frac{V_{\mathrm{CNT}}}{G_{12}^{\mathrm{CNT}}} + \frac{V_m}{G^m}, \tag{4a–c}$$

where E_{11}^{CNT}, E_{22}^{CNT} and G_{12}^{CNT} are the Young's and shear moduli of the carbon nanotubes corresponding to their principal material coordinates, respectively; E^{m} and G^{m} are, respectively, the Young's and shear moduli of the matrix; and $\eta_j (j = 1, 2, 3)$ denote the efficiency parameters of CNTs. Moreover, V_{CNT} and V_{m} are, respectively, the volume fractions of the CNTs and matrix with the condition of $V_{\mathrm{CNT}} + V_{\mathrm{m}} = 1$.

3 Equations of motion and boundary conditions

In this study, the thin-to-moderately thick FG-CNTRC skewed cylindrical panels are considered. In order to include the influences of the transverse shear deformation and rotary inertia, the first-order shear deformation theory of shells is used to model the variation of the displacement components along the panel thickness. Accordingly, the displacement components $\hat{u}$, $\hat{v}$ and $\hat{w}$ of an arbitrary material point (x, s, z) along the x-, s- and z-directions can be approximated as follows:

$$\hat{u}(x, s, z, t) = u(x, s, t) + z\phi^x(x, s, t), \quad \hat{v}(x, s, z, t) = v(x, s, t) + z\phi^s(x, s, t), \quad \hat{w}(x, s, z, t) = w(x, s, t). \tag{5a–c}$$

In the above relations, u, v and w represent the displacement components of a material point (x,s) on the mid-plane of the panel along the x-,s- and z-directions, respectively; also, ϕ^x and ϕ^s are the rotation components of the transverse normal at the material point (x, s) on the mid-plane of the panel about the s- and x-axes, respectively.

Based on the linear elasticity theory, the nonzero linear strain components (ε_{xx}, ε_{ss}, γ_{xs}, γ_{sz}, γ_{xz}) in terms of the displacement components can be written as [73,74]

$$\varepsilon_{xx} = \frac{\partial\hat{u}}{\partial x}, \quad \varepsilon_{ss} = \frac{\partial\hat{v}}{\partial s} + \frac{\hat{w}}{R}, \quad \gamma_{xs} = \frac{\partial\hat{v}}{\partial x} + \frac{\partial\hat{u}}{\partial s}, \quad \gamma_{sz} = \frac{\partial\hat{v}}{\partial z} + \frac{\partial\hat{w}}{\partial s} - \frac{\hat{v}}{R}, \quad \gamma_{xz} = \frac{\partial\hat{u}}{\partial z} + \frac{\partial\hat{w}}{\partial x}. \tag{6a–e}$$

Also, according to the FSDT of shells, the constitutive relations of the FG-CNTRC cylindrical panels can be stated as [74,75]

$$\begin{Bmatrix} \sigma_{xx} \\ \sigma_{ss} \\ \sigma_{xs} \\ \sigma_{xz} \\ \sigma_{sz} \end{Bmatrix} = \begin{bmatrix} Q_{11} & Q_{12} & 0 & 0 & 0 \\ Q_{12} & Q_{22} & 0 & 0 & 0 \\ 0 & 0 & Q_{66} & 0 & 0 \\ 0 & 0 & 0 & Q_{55} & 0 \\ 0 & 0 & 0 & 0 & Q_{44} \end{bmatrix} \begin{Bmatrix} \varepsilon_{xx} \\ \varepsilon_{ss} \\ \gamma_{xs} \\ \gamma_{xz} \\ \gamma_{sz} \end{Bmatrix}, \tag{7}$$

where $(\sigma_{xx}, \sigma_{yy}, \sigma_{xy}, \sigma_{xz}, \sigma_{sz})$ are the stress tensor components and Q_{ij}'s are the elastic constants, which for an orthotropic material are related to Young's modulus E_{ij} $(i, j = 1, 2)$, Poisson's ratio $\nu_{ij}(z)(i, j = 1, 2, i \neq j)$ and shear modulus $G_{ij}(z)(i, j = 1, 2, 3, i \neq j)$ as follows:

$$Q_{11} = \frac{E_{11}(z)}{1 - \nu_{12}(z)\,\nu_{21}(z)}, \quad Q_{12} = \frac{E_{12}(z)\,\nu_{12}(z)}{1 - \nu_{12}(z)\,\nu_{21}(z)}, \quad Q_{22} = \frac{E_{22}(z)}{1 - \nu_{12}(z)\,\nu_{21}(z)}, \quad Q_{44} = k_{\mathrm{s}}G_{23}(z), \tag{8a–f}$$

$$Q_{55} = k_{\mathrm{s}}G_{13}(z), \quad Q_{66} = G_{12}(z),$$

where k_s is the shear correction factor.

The governing differential equations of motion together with the related boundary conditions are derived by using Hamilton's principle, which in the case of free vibration analysis takes the following form:

$$\int_{t_1}^{t_2} (\delta U - \delta T)\mathrm{d}t = 0, \tag{9}$$

where the symbol δ is the variational operator; t is the temporal variable; t_1 and t_2 are two arbitrary times; δU and δT are the variations of the strain potential energy and kinetic energy of the FG-CNTRC panel, respectively. Based on the FSDT of shells, the variation of the strain energy over the volume V of the panel can be stated as

$$\delta U = \int_V \left(\sigma_{xx}\delta\varepsilon_{xx} + \sigma_{ss}\delta\varepsilon_{ss} + \sigma_{xs}\delta\gamma_{xs} + \sigma_{xz}\delta\gamma_{xz} + \sigma_{sz}\delta\gamma_{sz}\right)\mathrm{d}V. \tag{10}$$

Also, the variation of the kinetic energy is given by

$$\delta T = \int_V \rho\left[\frac{\partial\hat{u}}{\partial t}\frac{\partial\left(\delta\hat{u}\right)}{\partial t} + \frac{\partial\hat{v}}{\partial t}\frac{\partial\left(\delta\hat{v}\right)}{\partial t} + \frac{\partial w}{\partial t}\frac{\partial\left(\delta w\right)}{\partial t}\right]\mathrm{d}V. \tag{11}$$

Using Eqs. (5)–(11), the governing differential equations of motion can be expressed by doing some mathematical manipulations as follows:

$$\begin{aligned}
&\delta u\colon A_{11}\frac{\partial^2 u}{\partial x^2} + A_{66}\frac{\partial^2 u}{\partial s^2} + (A_{12}+A_{66})\frac{\partial^2 v}{\partial s\partial x} + \frac{A_{12}}{R}\frac{\partial w}{\partial x} + B_{11}\frac{\partial^2\varphi^x}{\partial x^2}\\
&\quad + B_{66}\frac{\partial^2\varphi^x}{\partial s^2} + (B_{12}+B_{66})\frac{\partial^2\varphi^s}{\partial s\partial x} = \hat{I}_0\frac{\partial^2 u}{\partial t^2} + \hat{I}_1\frac{\partial^2\varphi^x}{\partial t^2}
\end{aligned} \tag{12}$$

$$\begin{aligned}
&\delta v\colon (A_{12}+A_{66})\frac{\partial^2 u}{\partial x\partial s} + A_{22}\frac{\partial^2 v}{\partial s^2} + A_{66}\frac{\partial^2 v}{\partial x^2} - \frac{A_{44}}{R^2}v + \frac{1}{R}(A_{22}+A_{44})\frac{\partial w}{\partial s}\\
&\quad + (B_{12}+B_{66})\frac{\partial^2\varphi^x}{\partial x\partial s} + B_{22}\frac{\partial^2\varphi^s}{\partial s^2} + B_{66}\frac{\partial^2\varphi^s}{\partial x^2} + \frac{A_{44}}{R}\varphi^s = \hat{I}_0\frac{\partial^2 v}{\partial t^2} + \hat{I}_1\frac{\partial^2\varphi^s}{\partial t^2}
\end{aligned} \tag{13}$$

$$\begin{aligned}
&\delta w\colon -\frac{A_{12}}{R}\frac{\partial u}{\partial x} - \frac{1}{R}(A_{22}+A_{44})\frac{\partial v}{\partial s} + A_{55}\frac{\partial^2 w}{\partial x^2} + A_{44}\frac{\partial^2 w}{\partial s^2} - \frac{A_{22}}{R^2}w\\
&\quad + \left(A_{55} - \frac{B_{12}}{R}\right)\frac{\partial\varphi^x}{\partial x} + \left(A_{44} - \frac{B_{22}}{R}\right)\frac{\partial\varphi^s}{\partial s} = \hat{I}_0\frac{\partial^2 w}{\partial t^2}
\end{aligned} \tag{14}$$

$$\begin{aligned}
&\delta\varphi^x\colon B_{11}\frac{\partial^2 u}{\partial x^2} + B_{66}\frac{\partial^2 u}{\partial s^2} + (B_{12}+B_{66})\frac{\partial^2 v}{\partial s\partial x} - \left(A_{55} - \frac{B_{66}}{R}\right)\frac{\partial w}{\partial x} + D_{11}\frac{\partial^2\varphi^x}{\partial x^2}\\
&\quad + D_{66}\frac{\partial^2\varphi^x}{\partial s^2} - A_{55}\varphi^x + (D_{66}+D_{12})\frac{\partial^2\varphi^s}{\partial s\partial x} = \hat{I}_1\frac{\partial^2 u}{\partial t^2} + \hat{I}_2\frac{\partial^2\varphi^x}{\partial t^2}
\end{aligned} \tag{15}$$

$$\begin{aligned}
&\delta\varphi^s\colon (B_{12}+B_{66})\frac{\partial^2 u}{\partial x\partial s} + B_{66}\frac{\partial^2 v}{\partial x^2} + B_{22}\frac{\partial^2 v}{\partial s^2} + \frac{A_{44}}{R}v - \left(A_{44} - \frac{B_{22}}{R}\right)\frac{\partial w}{\partial s}\\
&\quad + (D_{12}+D_{66})\frac{\partial^2\varphi^x}{\partial x\partial s} + D_{22}\frac{\partial^2\varphi^s}{\partial s^2} + D_{66}\frac{\partial^2\varphi^s}{\partial x^2} - A_{44}\varphi^s = \hat{I}_1\frac{\partial^2 v}{\partial t^2} + \hat{I}_2\frac{\partial^2\varphi^s}{\partial t^2}
\end{aligned} \tag{16}$$

where

$$\left[A_{ij} \quad B_{ij} \quad D_{ij}\right] = \int_{-\frac{h}{2}}^{\frac{h}{2}} Q_{ij}\left[1 \quad z \quad z^2\right]\mathrm{d}z \quad \text{for } (i,j=1,2,6), \quad A_{ij} = \kappa_s\int_{-\frac{h}{2}}^{\frac{h}{2}} Q_{ij}\mathrm{d}z \quad \text{for } (i,j=4,5), \tag{17a, b}$$

$$\left[\hat{I}_0 \quad \hat{I}_1 \quad \hat{I}_2\right] = \int_{-\frac{h}{2}}^{\frac{h}{2}} \rho\left[1 \quad z \quad z^2\right]\mathrm{d}z. \tag{18}$$

Different types of the classical boundary conditions can be considered for the vibration of the FG-CNTRC skewed panels. The most common ones that are considered in the literature are in the following forms:

In-plane immovable or hard simply supported (S):

$$w = 0, \quad u = 0, \quad v = 0, \quad -n_s\varphi^x + n_x\varphi^s = 0, \quad M_{nn} = n_x^2 M_{xx} + 2n_x n_s M_{xs} + n_s^2 M_{ss} = 0 \tag{19a–e}$$

In-plane movable or soft simply supported (S^*):

$$w = 0, \quad -n_s u + n_x v = 0, \quad -n_s\varphi^x + n_x\varphi^s = 0, \quad N_{nn} = n_x^2 N_{xx} + 2n_x n_s N_{xs} + n_s^2 N_{ss} = 0, \tag{20a–e}$$
$$M_{nn} = n_x^2 M_{xx} + 2n_x n_s M_{xs} + n_s^2 M_{ss} = 0$$

Clamped (C):

$$w = 0, \quad u = 0, \quad v = 0, \quad \varphi^x = 0, \quad \varphi^s = 0 \tag{21a–e}$$

Free (F):

$$N_{nn} = n_x^2 N_{xx} + 2n_x n_s N_{xs} + n_s^2 N_{ss} = 0, N_{ns} = \left(n_x^2 - n_s^2\right) N_{xs} + n_x n_s \left(N_{xx} - N_{ss}\right) = 0, \tag{22a–e}$$
$$M_{nn} = n_x^2 M_{xx} + 2n_x n_s M_{xs} + n_s^2 M_{ss} = 0, M_{ns} = \left(n_x^2 - n_s^2\right) M_{xs} + n_x n_s \left(M_{xx} - M_{ss}\right) = 0,$$
$$Q_{nz} = n_x Q_{xz} + n_s Q_{sz} = 0$$

where

$$\begin{bmatrix} N_{xx} & M_{xx} \\ N_{ss} & M_{ss} \\ N_{xs} & M_{xs} \end{bmatrix} = \int_{-\frac{h}{2}}^{\frac{h}{2}} \begin{Bmatrix} \sigma_{xx} \\ \sigma_{ss} \\ \sigma_{xs} \end{Bmatrix} \begin{bmatrix} 1 & z \end{bmatrix} \mathrm{d}z, \quad \begin{bmatrix} Q_{xz} \\ Q_{sz} \end{bmatrix} = \int_{-\frac{h}{2}}^{\frac{h}{2}} \begin{Bmatrix} \sigma_{xz} \\ \sigma_{sz} \end{Bmatrix} \mathrm{d}z, \tag{23a, b}$$

where n_x and n_s are the x and s components of the unit normal to the skewed panel boundaries, respectively. In this study, the skewed panels with these types of boundary conditions and some combinations of them are analyzed.

4 The TDQM discretization algorithm

Recently, approximate numerical methods such as improved moving least squares-Ritz method [76,77], finite element method (FEM) [78] and mixed finite element-differential quadrature method [79] are used to solve the different complicated structural problems. On the other hand, it is necessary to develop a solution method with low computational cost and high accuracy for the case of skewed panels. The DQM as an efficient and accurate numerical tool has been used to study the skew and quadrilateral CNTRC plates in the past [35,42–46]. However, to the best of authors' knowledge, neither non-homogeneous nor homogeneous skewed panels have been analyzed by employing this method. Hence, in this work the applicability of the method is further demonstrated by solving the governing differential equations subjected to the related boundary conditions of the FG-CNTRC skewed cylindrical panels. In this regard, a new transformed weighting coefficients are introduced to make the discretization procedure of the governing equations more systematic for the case of the skewed cylindrical panels. For this purpose, firstly, a two-dimensional geometric transformation technique is applied between the skewed physical domain and the square computational domain to achieve the Jacobian transformation matrix of the skewed panels (see Fig. 2). Then, a systematic approach is constructed to express the derivatives in the physical domain (x, s) in term of the derivatives in the computational domain (ξ, η). The advantage of this procedure is the use of the transformed weighting coefficients in the physical domain (x, s) to discretize the differential equations without necessity to transform the governing differentials equations to the computational domain. The mapping between the physical and computational domains is expressed as follows (see Fig. 2):

$$x = a\xi + \left(R\theta_0 \tan\alpha\right)\eta, \quad s = R\theta_0\eta. \tag{24a, b}$$

The first-order global derivatives relation between the physical and computational domains can be expressed by using Eq. (24) in conjunction with the chain rules for an arbitrary function in terms of ξ and η coordinate variables as

$$\begin{Bmatrix} \frac{\partial\mu}{\partial x} \\ \frac{\partial\mu}{\partial s} \end{Bmatrix} = [T] \begin{Bmatrix} \frac{\partial\mu}{\partial\xi} \\ \frac{\partial\mu}{\partial\eta} \end{Bmatrix}, \tag{25}$$

where $\mu = (u, v, w, \varphi^x, \varphi^s)$ and

$$[T] = \begin{bmatrix} T_{11} & T_{12} \\ T_{21} & T_{22} \end{bmatrix} = \begin{bmatrix} \frac{\partial x}{\partial \xi} & \frac{\partial s}{\partial \xi} \\ \frac{\partial x}{\partial \eta} & \frac{\partial s}{\partial \eta} \end{bmatrix}^{-1} = \begin{bmatrix} a & 0 \\ R\theta_0 \tan\alpha & R\theta_0 \end{bmatrix}. \tag{26}$$

On the other hand, the derivatives of a function with respect to a space variable are approximated by the GDQ method. Accordingly, the first-order derivatives of a function μ at a given grid point (ξ_i, η_j) can be approximated as [80–82]

$$\left(\frac{\partial \mu}{\partial \xi}\right)_{(\xi_i,\eta_j)} = \sum_{p=1}^{N_\xi}\sum_{q=1}^{N_\eta} A_{ip}^{\xi} I_{jq}^{\eta} \mu\left(\xi_p, \eta_q\right) = \sum_{p=1}^{N_\xi}\sum_{q=1}^{N_\eta} A_{ip}^{\xi} I_{jq}^{\eta} \mu_{pq}, \quad \left(\frac{\partial \mu}{\partial \eta}\right)_{(\xi_i,\eta_j)} = \sum_{p=1}^{N_\xi}\sum_{q=1}^{N_\eta} I_{ip}^{\xi} A_{jq}^{\eta} \mu_{pq} \tag{27a, b}$$

$$\text{for } i = 1, \ldots, N_\xi \quad \text{and} \quad j = 1, \ldots, N_\eta,$$

where $A_{ij}^{\alpha}(\alpha = \xi, \eta)$ are the weighting coefficients of the first-order derivative in the computational domain corresponding to the coordinate variable $\alpha(= \xi, \eta)$; N_ξ and N_η denote the number of grid points along the ξ and η directions, respectively; also, I_{ij}^{ξ} and I_{ij}^{η} are the elements of the identity matrices of order N_ξ and N_η, respectively.

Substituting Eq. (27) into Eq. (25) one obtains

$$\left(\frac{\partial \mu}{\partial x}\right)_{ij} = \sum_{p=1}^{N_x=N_\xi}\sum_{q=1}^{N_{sy}=N_\eta} \left[(T_{11})_{ij}\, A_{ip}^{\xi} I_{jq}^{\eta} + (T_{12})_{ij}\, I_{ip}^{\xi} A_{jq}^{\eta}\right] \mu_{pq}, \tag{28a, b}$$

$$\left(\frac{\partial \mu}{\partial s}\right)_{ij} = \sum_{p=1}^{N_x=N_\xi}\sum_{q=1}^{N_{sy}=N_\eta} \left[(T_{21})_{ij}\, A_{ip}^{\xi} I_{jq}^{\eta} + (T_{22})_{ij}\, I_{ip}^{\xi} A_{jq}^{\eta}\right] \mu_{pq}.$$

On the other hand,

$$\left(\frac{\partial \mu}{\partial x}\right)_{ij} = \sum_{p=1}^{N_x=N_\xi}\sum_{q=1}^{N_{sy}=N_\eta} \tilde{A}_{ipjq}^{x} \mu_{pq}, \quad \left(\frac{\partial \mu}{\partial s}\right)_{ij} = \sum_{p=1}^{N_x=N_\xi}\sum_{q=1}^{N_{sy}=N_\eta} \tilde{A}_{ipjq}^{s} \mu_{pq}. \tag{29a, b}$$

By comparing Eqs. (28) and (29), the transformed weighting coefficients of the TDQM for the first-order derivatives are obtained as

$$\tilde{A}_{ipjq}^{x} = (T_{11})_{ij}\, A_{ip}^{\xi} I_{jq}^{\eta} + (T_{12})_{ij}\, I_{ip}^{\xi} A_{jq}^{\eta}, \quad \tilde{A}_{ipjq}^{s} = (T_{21})_{ij}\, A_{ip}^{\xi} I_{jq}^{\eta} + (T_{22})_{ij}\, I_{ip}^{\xi} A_{jq}^{\eta}. \tag{30a, b}$$

Also, according to the TDQM, the second-order derivatives can be written as

$$\left(\frac{\partial^2 \mu}{\partial x^2}\right)_{ij} = \sum_{p=1}^{N_x=N_\xi}\sum_{q=1}^{N_{sy}=N_\eta} \tilde{B}_{ipjq}^{x} \mu_{pq}, \quad \left(\frac{\partial^2 \mu}{\partial s^2}\right)_{ij} = \sum_{p=1}^{N_x=N_\xi}\sum_{q=1}^{N_{sy}=N_\eta} \tilde{B}_{ipjq}^{s} \mu_{pq}, \tag{31a–c}$$

$$\left(\frac{\partial^2 \mu}{\partial x \partial s}\right)_{ij} = \sum_{p=1}^{N_x=N_\xi}\sum_{q=1}^{N_{sy}=N_\eta} \tilde{B}_{ipjq}^{xs} \mu_{pq}.$$

By using Eq. (30), it can be easily shown that the transformed weighing coefficients for the second-order derivatives can be expressed as

$$\tilde{B}_{ipjq}^{x} = \sum_{k=1}^{N_x}\sum_{l=1}^{N_s} \tilde{A}_{ikjl}^{x} \tilde{A}_{kplq}^{x}, \quad \tilde{B}_{ipjq}^{xs} = \sum_{k=1}^{N_x}\sum_{l=1}^{N_s} \tilde{A}_{ikjl}^{x} \tilde{A}_{kplq}^{s}, \quad \tilde{B}_{ipjq}^{s} = \sum_{k=1}^{N_x}\sum_{l=1}^{N_s} \tilde{A}_{ikjl}^{s} \tilde{A}_{kplq}^{s}. \tag{32a–c}$$

Using the above-mentioned rule of derivative discretization of the present transformed differential quadrature (TDQ) method, the equations of motion at an arbitrary domain grid point (x_i, s_j) can be discretized as follows:

Equation (12):

$$\sum_{p=1}^{N_\xi}\sum_{q=1}^{N_\eta}\Big[\Big(A_{11}\tilde{B}^x_{ipjq}+A_{66}\tilde{B}^s_{ipjq}\Big)u_{pq}+\Big((A_{12}+A_{66})\tilde{B}^{xs}_{ipjq}\Big)v_{pq}+\frac{A_{12}}{R}\tilde{A}^x_{ipjq}w_{pq}$$
$$+\Big(B_{11}\tilde{B}^x_{ipjq}+B_{66}\tilde{B}^s_{ipjq}\Big)\varphi^x_{pq}+\Big((B_{12}+B_{66})\tilde{B}^{xs}_{ipjq}\Big)\varphi^s_{pq}\Big]=\hat{I}_0\left(\frac{\mathrm{d}^2u}{\mathrm{d}t^2}\right)_{ij}+\hat{I}_1\left(\frac{\mathrm{d}^2\varphi^x}{\mathrm{d}t^2}\right)_{ij} \tag{33}$$

Equation (13):

$$\sum_{p=1}^{N_\xi}\sum_{q=1}^{N_\eta}\Big[\Big((A_{12}+A_{66})\tilde{B}^{xs}_{ipjq}\Big)u_{pq}+\Big(A_{22}\tilde{B}^x_{ipjq}+A_{66}\tilde{B}^s_{ipjq}-\frac{A_{44}}{R^2}I_{ipjq}\Big)v_{pq}+\frac{1}{R}(A_{22}+A_{44})\tilde{A}^s_{ipjq}w_{pq}$$
$$+\Big((B_{12}+B_{66})\tilde{B}^{xs}_{ipjq}\Big)\varphi^x_{pq}+\Big(B_{22}\tilde{B}^s_{ipjq}+B_{66}\tilde{B}^x_{ipjq}+\frac{A_{44}}{R}I_{ipjq}\Big)\varphi^s_{pq}\Big]=\hat{I}_0\left(\frac{\mathrm{d}^2v}{\mathrm{d}t^2}\right)_{ij}+\hat{I}_1\left(\frac{\mathrm{d}^2\varphi^s}{\mathrm{d}t^2}\right)_{ij} \tag{34}$$

Equation (14):

$$\sum_{p=1}^{N_\xi}\sum_{q=1}^{N_\eta}\Big[-\frac{A_{12}}{R}\tilde{A}^x_{ipjq}u_{pq}-\frac{1}{R}(A_{22}+A_{44})\tilde{A}^s_{ipjq}v_{pq}+\Big(A_{55}\tilde{B}^x_{ipjq}+A_{44}\tilde{B}^s_{ipjq}-\frac{A_{22}}{R^2}I_{ipjq}\Big)w_{pq}$$
$$+\Big(A_{55}-\frac{B_{12}}{R}\Big)\tilde{A}^x_{ipjq}\varphi^x_{pq}+\Big(A_{44}-\frac{B_{22}}{R}\Big)\tilde{A}^s_{ipjq}\varphi^s_{pq}\Big]=\hat{I}_0\left(\frac{\mathrm{d}^2w}{\mathrm{d}t^2}\right)_{ij} \tag{35}$$

Equation (15):

$$\sum_{p=1}^{N_\xi}\sum_{q=1}^{N_\eta}\Big[\Big(B_{11}\tilde{B}^x_{ipjq}+B_{66}\tilde{B}^s_{ipjq}\Big)u_{pq}+\Big((B_{12}+B_{66})\tilde{B}^{xs}_{ipjq}\Big)v_{pq}+\Big(A_{55}-\frac{B_{66}}{R}\Big)\tilde{A}^x_{ipjq}w_{pq}$$
$$+\Big(D_{11}\tilde{B}^x_{ipjq}+D_{66}\tilde{B}^s_{ipjq}-A_{55}I_{ipjq}\Big)\varphi^x_{pq}+\Big((D_{12}+D_{66})\tilde{B}^{xs}_{ipjq}\Big)\varphi^s_{pq}\Big]=\hat{I}_1\left(\frac{\mathrm{d}^2u}{\mathrm{d}t^2}\right)_{ij}+\hat{I}_2\left(\frac{\mathrm{d}^2\varphi^x}{\mathrm{d}t^2}\right)_{ij} \tag{36}$$

Equation (16):

$$\sum_{p=1}^{N_\xi}\sum_{q=1}^{N_\eta}\Big[\Big((B_{12}+B_{66})\tilde{B}^{xs}_{ipjq}\Big)u_{pq}+\Big(B_{22}\tilde{B}^s_{ipjq}+B_{66}\tilde{B}^x_{ipjq}+\frac{A_{44}}{R}I_{ipjq}\Big)v_{pq}-\Big(A_{44}-\frac{B_{22}}{R}\Big)\tilde{A}^s_{ipjq}w_{pq}$$
$$+\Big((D_{12}+D_{66})\tilde{B}^{xs}_{ipjq}\Big)\varphi^x_{pq}+\Big(D_{22}\tilde{B}^s_{ipjq}+D_{66}\tilde{B}^x_{ipjq}-A_{44}I_{ipjq}\Big)\varphi^s_{pq}\Big]=\hat{I}_1\left(\frac{\mathrm{d}^2v}{\mathrm{d}t^2}\right)_{ij}+\hat{I}_2\left(\frac{\mathrm{d}^2\varphi^s}{\mathrm{d}t^2}\right)_{ij} \tag{37}$$

where $I_{ipjq}=I^{\xi}_{ip}I^{\eta}_{jq}$. In a similar manner, the related boundary conditions can be discretized at the boundary grid points (x_i, s_j). Here, for brevity, the discretized form of the immoveable simply supported and free boundary conditions along the edges $\xi=0$ and 1 are presented and the other types of boundary conditions can be discretized in a similar manner.

Immoveable simply supported boundary conditions (S):

$$w_{b_\xi j}=0,\quad u_{b_\xi j}=0,\quad v_{b_\xi j}=0,\quad -n_s\varphi^x_{b_\xi j}+n_x\varphi^s_{b_\xi j}=0,$$

$$\begin{aligned}M_{nn}=\sum_{p=1}^{N_\xi}\sum_{q=1}^{N_\eta}\Big[&n_x^2\left(B_{11}\tilde{A}^x_{b_\xi pjq}\,u_{pq}+D_{11}\tilde{A}^x_{b_\xi pjq}\varphi^x_{pq}\right.\\&\left.+B_{12}\tilde{A}^s_{b_\xi pjq}v_{pq}+D_{12}\tilde{A}^s_{b_\xi pjq}\varphi^s_{pq}+\frac{B_{12}}{R}I_{b_\xi pjq}w_{pq}\right)+n_s^2\left(B_{12}\tilde{A}^x_{b_\xi pjq}u_{pq}+D_{12}\tilde{A}^x_{b_\xi pjq}\varphi^x_{pq}\right.\\&\left.+B_{22}\tilde{A}^s_{b_\xi pjq}v_{pq}+D_{22}\tilde{A}^s_{b_\xi pjq}\varphi^s_{pq}+\frac{B_{22}}{R}I_{b_\xi pjq}w_{pq}\right)+2n_xn_s\left(B_{66}\tilde{A}^s_{b_\xi pjq}u_{pq}+D_{66}\tilde{A}^s_{b_\xi pjq}\varphi^x_{pq}\right.\\&\left.+B_{66}\tilde{A}^x_{b_\xi pjq}v_{pq}+D_{66}\tilde{A}^x_{b_\xi pjq}\varphi^s_{pq}\right)\Big]=0\quad\text{for } j=2,3,\ldots,N_\eta-1\quad\text{and}\quad b_\xi=1\quad\text{or}\quad N_\xi\end{aligned}\tag{38a–e}$$

Free boundary conditions (F):

$$\begin{aligned}M_{nn}=\sum_{p=1}^{N_\xi}\sum_{q=1}^{N_\eta}\Big[&n_x^2\left(B_{11}\tilde{A}^x_{b_\xi pjq}\,u_{pq}+D_{11}\tilde{A}^x_{b_\xi pjq}\varphi^x_{pq}+\;B_{12}\tilde{A}^s_{b_\xi pjq}v_{pq}+D_{12}\tilde{A}^s_{b_\xi pjq}\varphi^s_{pq}+\frac{B_{12}}{R}I_{b_\xi pjq}w_{pq}\right)\\&+n_s^2\left(B_{12}\tilde{A}^x_{b_\xi pjq}u_{pq}+D_{12}\tilde{A}^x_{b_\xi pjq}\varphi^x_{pq}+B_{22}\tilde{A}^s_{b_\xi pjq}v_{pq}+D_{22}\tilde{A}^s_{b_\xi pjq}\varphi^s_{pq}+\frac{B_{22}}{R}I_{b_\xi pjq}w_{pq}\right)\\&+2n_xn_s\left(A_{66}\tilde{A}^s_{b_\xi pjq}u_{pq}+B_{66}\tilde{A}^s_{b_\xi pjq}\varphi^x_{pq}+A_{66}\tilde{A}^x_{b_\xi pjq}v_{pq}+B_{66}\tilde{A}^x_{b_\xi pjq}\varphi^s_{pq}\right)\Big]=0\end{aligned}\tag{39a}$$

$$\begin{aligned}M_{ns}=\sum_{p=1}^{N_\xi}\sum_{q=1}^{N_\eta}\Big[&n_xn_s\left(B_{11}\tilde{A}^x_{b_\xi pjq}\,u_{pq}+D_{11}\tilde{A}^x_{b_\xi pjq}\varphi^x_{pq}+B_{12}\tilde{A}^s_{b_\xi pjq}v_{pq}+D_{12}\tilde{A}^s_{b_\xi pjq}\varphi^s_{pq}+\frac{B_{12}}{R}I_{b_\xi pjq}w_{pq}\right)\\&-n_xn_s\left(B_{12}\tilde{A}^x_{b_\xi pjq}u_{pq}+D_{12}\tilde{A}^x_{b_\xi pjq}\varphi^x_{pq}+B_{22}\tilde{A}^s_{b_\xi pjq}v_{pq}+D_{22}\tilde{A}^s_{b_\xi pjq}\varphi^s_{pq}+\frac{B_{22}}{R}I_{b_\xi pjq}w_{pq}\right)\\&+\left(n_x^2-n_s^2\right)\left(B_{66}\tilde{A}^s_{b_\xi pjq}u_{pq}+D_{66}\tilde{A}^s_{b_\xi pjq}\varphi^x_{pq}+B_{66}\tilde{A}^x_{b_\xi pjq}v_{pq}+D_{66}\tilde{A}^x_{b_\xi pjq}\varphi^s_{pq}\right)\Big]=0\end{aligned}\tag{39b}$$

$$\begin{aligned}N_{nn}=\sum_{p=1}^{N_\xi}\sum_{q=1}^{N_\eta}\Big[&n_x^2\left(A_{11}\tilde{A}^x_{b_\xi pjq}\,u_{pq}+B_{11}\tilde{A}^x_{b_\xi pjq}\varphi^x_{pq}+A_{12}\tilde{A}^s_{b_\xi pjq}v_{pq}+B_{12}\tilde{A}^s_{b_\xi pjq}\varphi^s_{pq}+\frac{A_{12}}{R}I_{b_\xi pjq}w_{pq}\right)\\&+n_s^2\left(A_{12}\tilde{A}^x_{b_\xi pjq}u_{pq}+B_{12}\tilde{A}^x_{b_\xi pjq}\varphi^x_{pq}+A_{22}\tilde{A}^s_{b_\xi pjq}v_{pq}+B_{22}\tilde{A}^s_{b_\xi pjq}\varphi^s_{pq}+\frac{A_{22}}{R}I_{b_\xi pjq}w_{pq}\right)\\&+2n_xn_s\left(A_{66}\tilde{A}^s_{b_\xi pjq}u_{pq}+A_{66}\tilde{A}^s_{b_\xi pjq}\varphi^x_{pq}+A_{66}\tilde{A}^x_{b_\xi pjq}v_{pq}+A_{66}\tilde{A}^x_{b_\xi pjq}\varphi^s_{pq}\right)\Big]=0\end{aligned}\tag{39c}$$

$$\begin{aligned}N_{ns}=\sum_{p=1}^{N_\xi}\sum_{q=1}^{N_\eta}\Big[&n_xn_s\left(A_{11}\tilde{A}^x_{b_\xi pjq}\,u_{pq}+B_{11}\tilde{A}^x_{b_\xi pjq}\varphi^x_{pq}+A_{12}\tilde{A}^s_{b_\xi pjq}v_{pq}+B_{12}\tilde{A}^s_{b_\xi pjq}\varphi^s_{pq}+\frac{A_{12}}{R}I_{b_\xi pjq}w_{pq}\right)\\&-n_xn_s\left(A_{12}\tilde{A}^x_{b_\xi pjq}u_{pq}+B_{12}\tilde{A}^x_{b_\xi pjq}\varphi^x_{pq}+A_{22}\tilde{A}^s_{b_\xi pjq}v_{pq}+B_{22}\tilde{A}^s_{b_\xi pjq}\varphi^s_{pq}+\frac{A_{22}}{R}I_{b_\xi pjq}w_{pq}\right)\\&+\left(n_x^2-n_s^2\right)\left(A_{66}\tilde{A}^s_{b_\xi pjq}u_{pq}+A_{66}\tilde{A}^s_{b_\xi pjq}\varphi^x_{pq}+A_{66}\tilde{A}^x_{b_\xi pjq}v_{pq}+A_{66}\tilde{A}^x_{b_\xi pjq}\varphi^s_{pq}\right)\Big]=0\end{aligned}\tag{39d}$$

$$Q_{nz}=\sum_{p=1}^{N_\xi}\sum_{q=1}^{N_\eta}\left[n_xA_{55}\left(\tilde{A}^x_{b_\xi pjq}w_{pq}+\tilde{I}_{b_\xi pjq}\varphi^x_{pq}\right)+n_sA_{44}\left(\tilde{A}^s_{b_\xi pjq}w_{pq}-\frac{1}{R}\tilde{I}_{b_\xi pjq}v_{pq}+\tilde{I}_{b_\xi pjq}\varphi^s_{pq}\right)\right]=0\tag{39e}$$

The discretized equations of motion and the related boundary conditions in the matrix form can be written as:
Equations of motion:

$$[K_{db}]\{U_b\}+[K_{dd}]\{U_d\}+[M]\left\{\ddot{U}_d\right\}=\{0\}\tag{40}$$

Boundary conditions:

$$[K_{bb}]\{U_b\}+[K_{bd}]\{U_d\}=\{0\}\tag{41}$$

where $\{U_i\} = [\{u_i\}^{\mathrm{T}}\ \{v_i\}^T\ \{w_i\}^{\mathrm{T}}\ \{\varphi_i^x\}^{\mathrm{T}}\ \{\varphi_i^s\}^{\mathrm{T}}]^T$ with $(i = b, d)$ are the domain (d) and the boundary (b) degrees of freedom, respectively; $[K_{ij}]$ and $[M_{ij}]$ with $(i, j = b, d)$ are, respectively, the stiffness and mass matrices, and the dot means the derivative with respect to time t. Eliminating the boundary degrees of freedom from the system of Eq. (40) by using Eq. (41) and also considering the harmonic nature of the motion, one obtains a system of algebraic eigenvalue equations as

$$\left([K] - \omega^2 [M]\right) \left\{\hat{U}_d\right\} = \{0\}, \tag{42}$$

where $[K] = [K_{dd}] - [K_{db}][K_{bb}]^{-1}[K_{bd}]$, $[M] = [M_{dd}] - [M_{db}][K_{bb}]^{-1}[K_{bd}]$. Also, ω denotes the natural frequency of the panel and $\{\hat{U}_d\}$ represents the amplitude of motion. By solving the system of algebraic eigenvalue equations (42), the natural frequencies together with the corresponding mode shapes of the FG-CNTRC skewed cylindrical panels under different boundary conditions are obtained.

5 Numerical results

In this section, first of all, the convergence behavior of the presented formulation and the TDQM for the free vibration analysis of FG-CNTRC skewed cylindrical panels is studied. Then, a convergence and comparison study is carried out for FG-CNTRC skew plates (skew panel with large mean radius R) to establish the applicability and reliability of the approach. The accuracy of the numerical solution is further investigated by comparing the numerical results through two cases of the homogeneous skewed cylindrical panels and the FG-CNTRC rectangular panels with those available in the open literature. In addition, comparison studies for the FG-CNTRC skewed cylindrical panels with UD of CNTs are performed with those obtained via the finite element-based commercial software ANSYS. Afterward, the effects of the CNTs distributions and volume fractions, skew angles, aspect ratio, length-to-thickness ratio and different boundary conditions on the non-dimensional frequency parameter of the FG-CNTRC skewed cylindrical panels are presented.

In this study, the material properties which are used for the matrix (m) and reinforcing phase (CNTs) are, respectively, defined as [41], $\nu_m = 0.34$, $\rho_m = 1.15\,\mathrm{g/cm^3}$, $E_m = 2.1\,\mathrm{GPa}$, $E_{11}^{\mathrm{CNT}} = 5.6466\,\mathrm{TPa}$, $E_{22}^{\mathrm{CNT}} = 7.0800\,\mathrm{TPa}$, $G_{12}^{\mathrm{CNT}} = 1.9445\,\mathrm{TPa}$. The properties of the CNTs and matrix and are given at the room temperature of 300 K. The CNT efficiency parameters $\eta_j (j = 1, 2, 3)$ are adopted according to the reported effective properties of CNTRCs in literature (e.g., Ref. [83]) by matching the Young's moduli E_{11} and E_{22} with the counterparts computed by the rule of mixture. The material properties of the CNTRCs are presented in Table 1 which are chosen from the work of Shen [32]. Also, unless otherwise stated, the transverse shear correction factor is assumed to be $k_{\mathrm{s}} = 5/(6 - \nu_{12})$, which has been suggested for functionally graded materials [33] and it is assumed that $G_{23} = G_{13} = G_{12}$.

The edges of the FG-CNTRC skewed cylindrical panels are enumerated, respectively, from 1 to 4 as depicted in Fig. 2. For instance, S^*–C–F–S indicates that the edges 1–4 are, respectively, movable simply supported, clamped, free and immoveable simply supported. Also, the non-dimensional frequency parameter is defined to be $(\lambda_i = \omega_i (a^2/h)\sqrt{\rho_m/E_m})$, which is used in all numerical studies except those in Tables 3, 4, 5 and 6.

As a first example, the convergence behavior of the present approach for the free vibration analysis of fully clamped and simply supported FG-CNTRC skewed cylindrical panels is investigated and the results are shown in Table 2. The first three frequency parameters against the number of grid points are reported for the panels with FG-X distribution of CNTs. Also, Fig. 4 is provided to present the convergence behavior of the FG-CNTRC skewed cylindrical panels for various combinations of simply supported, clamped and free boundary conditions. The results of Table 2 and Fig. 4 are prepared for skewed panels with a sharp skew angle (i.e., $\alpha = 60°$) to better reflect the efficiency of the approach. The fast rate of convergence of the method for the FG-CNTRC skewed panels is quite evident. It can be seen that 17 grid points along the x and s-directions

Table 1 Material properties for a polymer composite reinforced by (10, 10) single-walled CNTs at room temperature [32]

V_{CNT}^*	E_{11} (GPa)	η_1	E_{22} (GPa)	η_2	η_3
0.11	94.4168	0.149	2.2037	0.934	0.934
0.14	120.3846	0.15	2.2977	0.941	0.941
0.17	144.7714	0.149	3.4939	1.381	1.381

Table 2 Convergence of the first three non-dimensional frequency parameters ($\lambda_i = \omega_i a^2/h\sqrt{\rho_m/E_m}$) of the FG-CNTRC skewed cylindrical panels with FG-X distribution of CNTs ($R/h = 10, a/h = 10, b/a = 1, \alpha = 60°, V^*_{\mathrm{CNT}} = 0.17$)

$N_\xi = N_\eta$	C–C–C–C			S–S–S–S		
	λ_1	λ_2	λ_3	λ_1	λ_2	λ_3
7	43.1379	62.1519	79.9991	32.8214	50.1634	69.4388
9	42.9701	59.8903	75.4305	32.8021	49.7842	65.6159
11	42.9603	59.8098	74.7486	32.8267	49.7688	65.4322
15	42.9575	59.8082	74.7293	32.8503	49.7720	65.4407
17	42.9572	59.8081	74.7292	32.8570	49.7730	65.4426
19	42.9571	59.8081	74.7291	32.8620	49.7737	65.4440
21	42.9570	59.8081	74.7291	32.8657	49.7741	65.4451
23	42.9569	59.8081	74.7291	32.8685	49.7745	65.4459

Table 3 Convergence and comparison study of the first three natural frequency parameters ($\bar{\lambda}_i = \omega_i a^2/(h\pi^2)\sqrt{\rho_m/E_m}$) and ($\bar{\omega}_i = \omega_i h\sqrt{2\rho_m(1+\nu_m)/E_m}$) of the fully clamped FG-CNTRC skew plates with UD of CNTs ($R/h = 1000, a/h = 10, b/a = 1$)

Source	N_ξ	($\alpha = 30°, V^*_{\mathrm{CNT}}$=0.17, $k_s = 5/6$)			($\alpha = 60°, V^*_{\mathrm{CNT}} = 0.17, k_s = 5/6$)		
		$\bar{\lambda}_1$	$\bar{\lambda}_2$	$\bar{\lambda}_3$	$\bar{\lambda}_1$	$\bar{\lambda}_2$	$\bar{\lambda}_3$
TDQ (present)	9	2.4129	3.3559	4.5509	4.0246	5.7146	7.2501
	11	2.4131	3.3556	4.5509	4.0236	5.7075	7.1853
	15	2.4131	3.3556	4.5510	4.0234	5.7073	7.1836
	17	2.4131	3.3556	4.5510	4.0233	5.7073	7.1836
DQM [35]		2.4131	3.3556	4.5510	4.0233	5.7073	7.1836
		($\alpha = 30°, V^*_{\mathrm{CNT}} = 0.14$)			($\alpha = 45°, V^*_{\mathrm{CNT}} = 0.14$)		
		$\bar{\omega}_1$	$\bar{\omega}_2$	$\bar{\omega}_3$	$\bar{\omega}_1$	$\bar{\omega}_2$	$\bar{\omega}_3$
TDQ (present)	7	0.3269	0.4596	0.6175	0.3808	0.5681	0.7197
	9	0.3270	0.4502	0.6172	0.3809	0.5539	0.7138
	11	0.3270	0.4502	0.6172	0.3809	0.5537	0.7134
DQM [45]		0.3271	0.4503	0.6173	0.3810	0.5538	0.7135

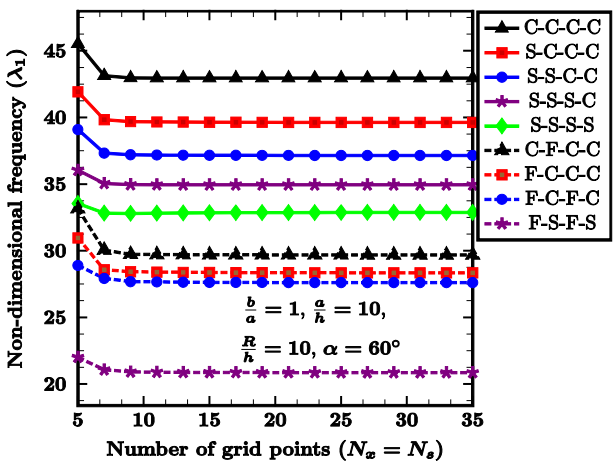

Fig. 4 Convergence behavior of non-dimensional fundamental frequency parameter for the FG-CNTRC skewed cylindrical panels with different boundary conditions (FG-X, $V^*_{\mathrm{CNT}} = 0.17$)

($N_x = N_s = 17$) lead the results with at least four digits convergence. Hence, these numbers of grid points are used for the following numerical calculations.

In Table 3, the accuracy of the numerical results is established through a convergence and comparison study of the first three non-dimensional frequency parameters of the fully clamped CNTRC skew plates as a limit case of the present formulation (i.e., when $R \to \infty$) with available published data in the literature. The comparison is performed with the DQM results of CNTRC skew plates obtained by Malekzadeh and Zarei

Table 4 Comparison of the first three non-dimensional frequency parameters ($\tilde{\lambda}_i = \omega_i R\sqrt{\rho/E}$) of the homogeneous skewed cylindrical shells with F–C–F–C (clamped at the curved edges) boundary condition ($a/R = 0.5$, $h/R = 0.05$, ν =0.3, $k_s = 5/6$, $E = 210\,\text{GPa}$, $\rho = 7800\,\text{kg/m}^3$)

Method	$\theta_0 = 30°$				$\theta_0 = 60°$			
	$\alpha = 0°$	$\alpha = 15°$	$\alpha = 30°$	$\alpha = 45°$	$\alpha = 0°$	$\alpha = 15°$	$\alpha = 30°$	$\alpha = 45°$
First mode ($\tilde{\lambda}_1$)								
TDQ	1.3019	1.3614	1.5649	1.9756	1.3505	1.4063	1.5903	1.9778
P-type [84]	1.314	1.375	1.585	2.006	1.365	1.423	1.616	2.020
I-DEAS [84]	1.307	1.366	1.567	1.979	1.356	1.405	1.565	1.901
Second mode ($\tilde{\lambda}_2$)								
TDQ	1.4441	1.4810	1.6194	1.9793	1.3693	1.4195	1.5935	1.9779
P-type [84]	1.462	1.500	1.643	2.014	1.383	1.435	1.614	2.020
I-DEAS [84]	1.452	1.489	1.626	1.981	1.375	1.419	1.563	1.901
Third mode ($\tilde{\lambda}_3$)								
TDQ	2.2411	2.2432	2.3096	2.7243	1.5948	1.6631	1.9147	2.5610
P-type [84]	2.269	2.271	2.340	2.772	1.609	1.678	1.935	2.602
I-DEAS [84]	2.272	2.274	2.338	2.746	1.601	1.667	1.912	2.538

Table 5 Comparison of the first three non-dimensional frequency parameters ($\tilde{\lambda}_i = \omega_i R\sqrt{\rho/E}$) of the homogeneous skewed cylindrical panels with F–C–F–C (clamped at the curved edges) boundary condition $\alpha = 45°$, $h/R = 0.01$, $\nu = 0.3$, $k_s = 5/6$, $E = 210\,\text{GPa}$, $\rho = 7800\,\text{kg/m}^3$)

Method	$\theta_0 = 30°$				$\theta_0 = 60°$			
	$a/R = 0.5$	$a/R = 1$	$a/R = 2$	$a/R = 3$	$a/R = 0.5$	$a/R = 1$	$a/R = 2$	$a/R = 3$
First mode ($\tilde{\lambda}_1$)								
TDQ	0.5016	0.1695	0.0553	0.0293	0.5016	0.1795	0.0733	0.0396
P-type [84]	0.505	0.170	0.056	0.030	0.509	0.181	0.074	0.040
I-DEAS [84]	0.500	0.169	0.055	0.029	0.484	0.177	0.073	0.039
Second mode ($\tilde{\lambda}_2$)								
TDQ	0.5020	0.1870	0.0655	0.0315	0.5017	0.1795	0.0761	0.0527
P-type [84]	0.505	0.188	0.066	0.032	0.509	0.181	0.076	0.053
I-DEAS [84]	0.500	0.187	0.066	0.031	0.484	0.178	0.076	0.053
Third mode ($\tilde{\lambda}_3$)								
TDQ	0.9096	0.3327	0.1215	0.0663	0.9233	0.3456	0.1298	0.0795
P-type [84]	0.913	0.334	0.122	0.067	0.930	0.349	0.130	0.080
I-DEAS [84]	0.909	0.332	0.121	0.066	0.900	0.341	0.129	0.079

[35] and Ansari et al. [45]. The results are prepared for different values of the skew angles and CNTs volume fraction. Excellent agreement between the numerical results can be observed which illustrates the accuracy of the solution method.

As another example, in Tables 4 and 5, the first three frequency parameters for the homogeneous skewed cylindrical panels are compared with those obtained by Kandasamy and Singh [84]. They used the finite element method to extract the results. The boundary conditions are free at the straight parallel edges and fully clamped at the curved edges. The results are presented for different values of the skew angle and length-to-radius ratio in Tables 4 and 5, respectively. As it can be seen, a very good agreement is achieved in all cases under consideration.

In order to validate the results of the present approach for the FG-CNTRC panels, the free vibration of FG-CNTRC rectangular panels with movable simply supported boundary conditions analyzed by Pouresmaeeli and Fazelzadeh [71] is considered. In Table 6, the obtained fundamental frequency parameters for different values of the CNTs volume fraction are compared with those reported in Ref. [71], which were extracted using Galerkin's method. The excellent agreements between the present numerical results and those of aforementioned solution are quite obvious, which indicate the accuracy of the present approach.

Through several examples, the present method proves to be reliable, efficient and accurate by performing convergence and comparison studies. At the next stage, the effects of various parameters on the non-dimensional frequency parameters of the FG-CNTRC skewed cylindrical panels are studied.

The influences of the CNTs distribution together with their volume fractions on the fundamental frequency parameters of the FG-CNTRC square and skewed cylindrical panels are presented in Tables 7 and 8,

Table 6 Comparison of the non-dimensional fundamental frequency parameter ($\lambda_1 = \omega_1 a^2/h\sqrt{\rho_m/E_m}$) of the FG-CNTRC square cylindrical panels with S^*–S^*–S^*–S^* boundary condition ($a/R = 0.5,\ a/h = 20, b/a = 1$)

Method	V^*_{CNT}	UD	FG-V	FG-X	FG-O
Present (TDQ)	0.11	18.0369	16.0357	20.5510	14.4072
Galerkin's method [71]		18.1263	16.0598	20.5479	14.5525
Present (TDQ)	0.14	19.6040	17.4066	22.2744	15.6476
Galerkin's method [71]		19.6278	17.3905	22.1792	15.7660
Present (TDQ)	0.17	22.3103	19.7952	25.5194	17.7691
Galerkin's method [71]		22.3797	19.7991	25.4877	17.9030

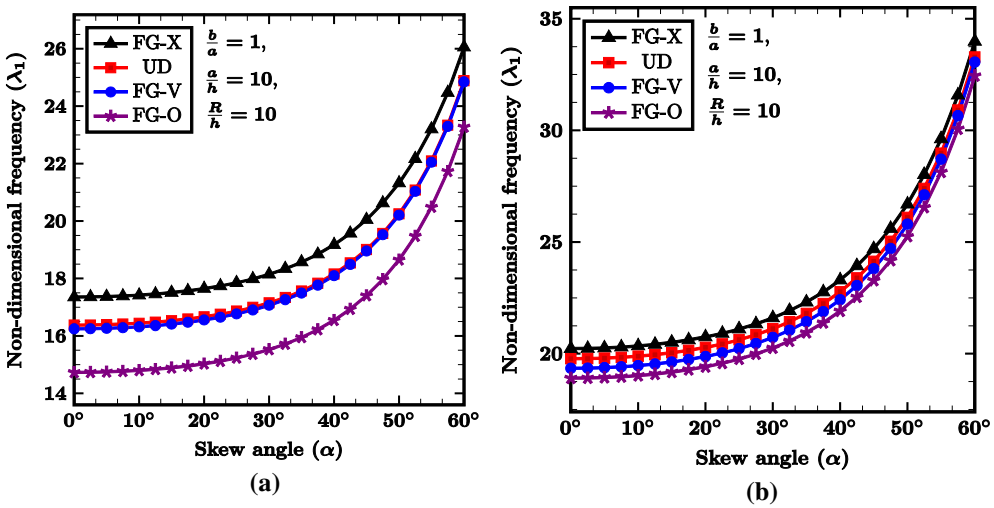

Fig. 5 **a**, **b** The variation of fundamental frequency parameter against the skew angle for the FG-CNTRC skewed cylindrical panels with different distribution of CNTs ($V^*_{CNT} = 0.11$), **a** simply supported, and **b** clamped

Table 7 Non-dimensional frequency parameters ($\lambda_i = \omega_i a^2/h\sqrt{\rho_m/E_m}$) of the FG-CNTRC square cylindrical panels with different volume fraction and CNTs distributions ($R/h = 10, \alpha = 0°, b/a = 1$)

V^*_{CNT}	a/h	C–C–C–C				S–S–S–S			
		UD	FG-V	FG-O	FG-X	UD	FG-V	FG-O	FG-X
0.11	10	19.774	19.347	18.903	20.228	16.378	16.247	14.731	17.354
	50	47.524	43.62	40.211	53.039	31.715	31.539	29.058	34.208
0.14	10	20.311	19.964	19.543	20.776	17.147	17.064	15.490	18.121
	50	50.979	46.563	42.764	57.028	33.361	33.145	30.170	36.346
0.17	10	24.683	24.205	23.592	25.418	20.381	20.327	18.325	21.713
	50	58.931	54.110	49.734	66.129	39.464	39.382	36.169	42.801

Table 8 Non-dimensional frequency parameters ($\lambda_i = \omega_i a^2/h\sqrt{\rho_m/E_m}$) of the FG-CNTRC skewed cylindrical panels with different volume fraction and CNTs distributions ($R/h = 10, b/a = 1, \alpha = 45°$)

V^*_{CNT}	a/h	C–C–C–C				S–S–S–S			
		UD	FG-V	FG-O	FG-X	UD	FG-V	FG-O	FG-X
0.11	10	24.137	23.806	23.282	24.695	19.008	18.958	17.402	20.050
	50	59.816	56.444	53.896	64.655	43.668	43.384	40.652	46.371
0.14	10	24.728	24.465	23.912	25.359	19.800	19.834	18.136	20.894
	50	63.083	59.278	56.330	68.510	45.438	45.193	41.924	48.687
0.17	10	30.146	29.810	28.991	31.146	23.675	23.815	21.606	25.184
	50	74.393	70.378	67.056	80.841	54.425	54.350	50.381	58.453

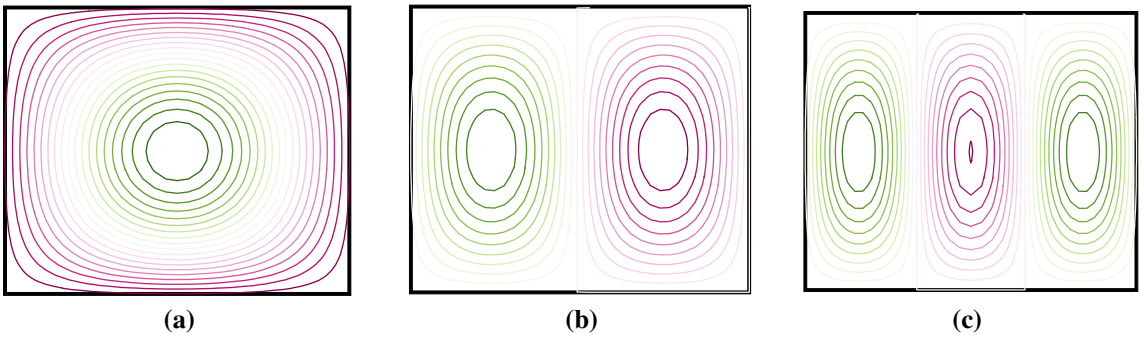

Fig. 6 **a–c** The first three mode shapes of a simply supported (S-S-S-S) FG-CNTRC cylindrical panel with UD of CNTs ($\alpha = 0°$), **a** first mode shape, **b** second mode shape, **c** third mode shape

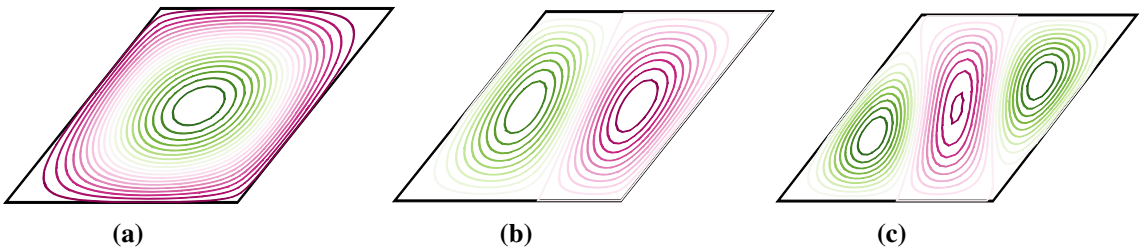

Fig. 7 **a–c** The first three mode shapes of a simply supported (S–S–S–S) CNTRC skewed cylindrical panel with UD of CNTs ($\alpha = 45°$), **a** first mode shape, **b** second mode shape, **c** third mode shape

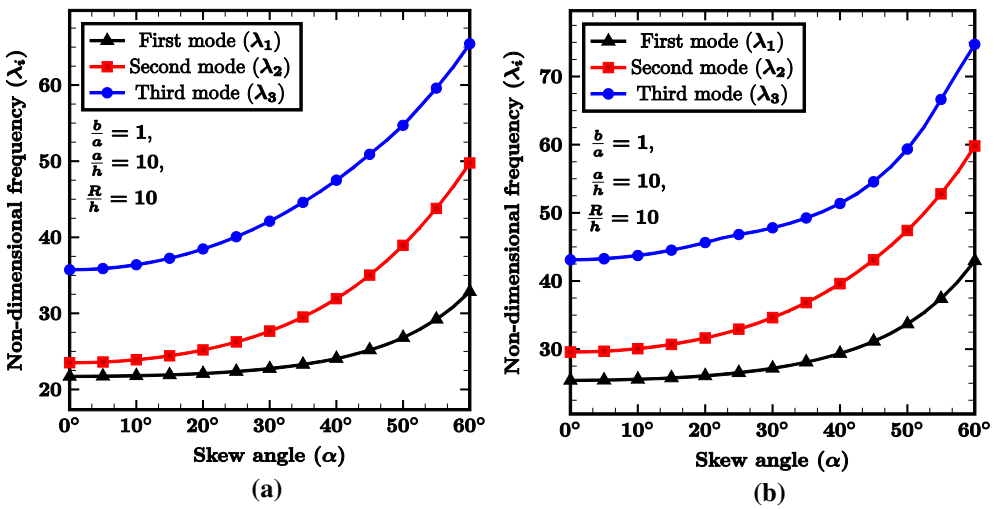

Fig. 8 **a**, **b** The variation of the first three frequency parameters versus skew angle for the FG-CNTRC skewed cylindrical panels ($V^*_{\mathrm{CNT}} = 0.17$, FG-X), **a** simply supported, and **b** clamped

respectively. The results are provided for the two different values of the length-to-thickness ratio of the panels, corresponding to moderately thick and thin panels, and also for the fully clamped and simply supported panels. It is observed that by a slight increase in the CNTs volume fraction, the frequency parameters change considerably. In Fig. 5, the influences of skew angles together with CNTs distributions on the fundamental frequency parameter of FG-CNTRC skewed panels are exhibited. From the data presented in Tables 7 and 8 and this figure, one can see that in all cases under consideration, the panels with the FG-X and FG-O distributions of the CNTs have the greatest and lowest natural frequencies, respectively. This means that the panels with FG-X distribution of CNTs show greater stiffness compared with the same panels but with other CNTs distributions. Also, the first three mode shapes of FG-CNTRC square and skewed cylindrical panels with UD of CNTs are,

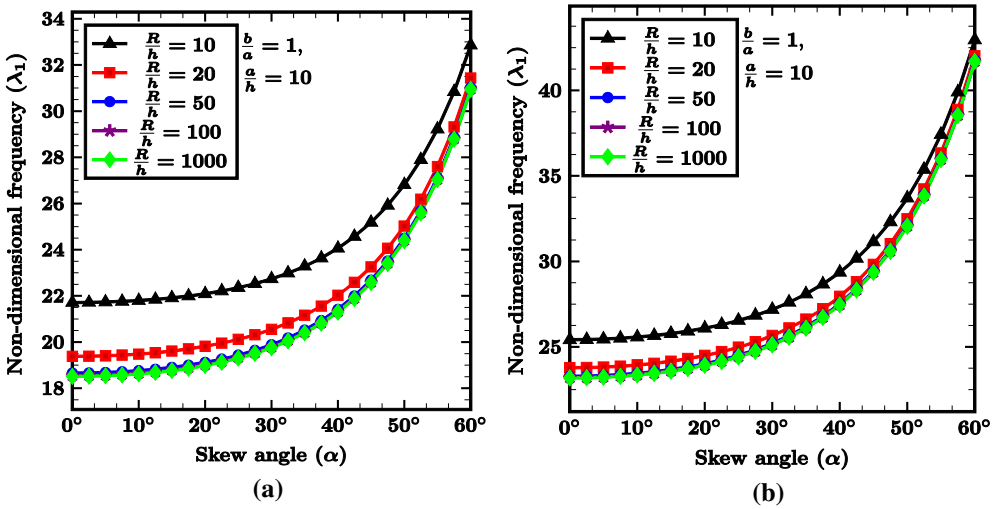

Fig. 9 **a**, **b** The variation of fundamental frequency parameter against the skew angle of FG-CNTRC skewed cylindrical panels for the five different radius-to-thickness ratios ($V^*_{\mathrm{CNT}} = 0.17$, FG-X), **a** simply supported, and **b** clamped

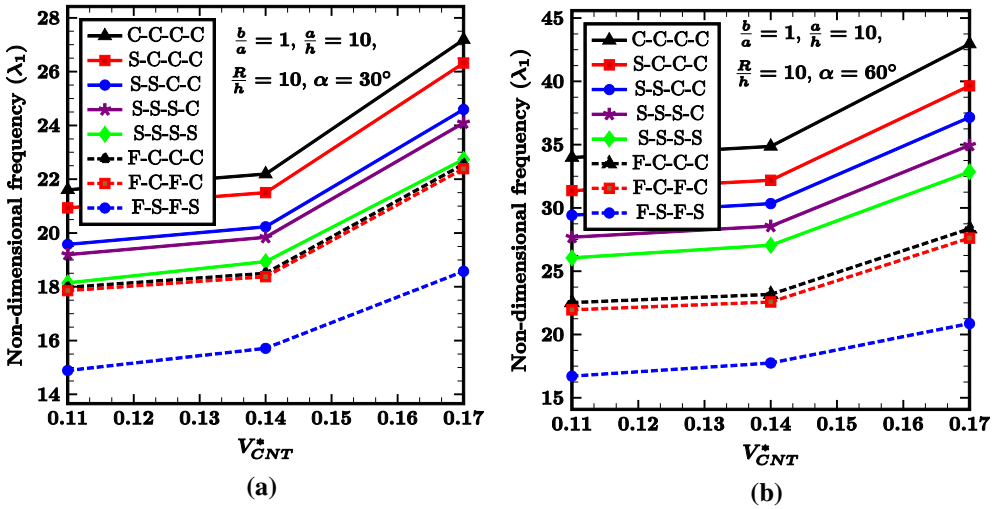

Fig. 10 **a**, **b** The influences of the boundary conditions on the variation of the fundamental frequency parameter versus CNTs volume fraction for the FG-CNTRC skewed cylindrical panels (FG-X), **a** $\alpha = 30°$, and **b** $\alpha = 60°$

respectively, depicted in Figs. 6 and 7. It can be seen that the skew angle only skewed the mode shapes and their overall behavior is the same for the skewed and square panels.

In Fig. 8, the variation of the first three frequency parameters versus the skew angle for the FG-CNTRC skewed cylindrical panels with FG-X distribution of CNTs is illustrated. Panels with both simply supported and fully clamped boundary conditions are considered. In all cases, it is observed that the frequency parameters increase monotonically as the skew angle increases. In addition, it can be seen that the skew angle plays a significant role on the higher natural frequencies of the FG-CNTRC skewed cylindrical panels.

The effects of skew angle together with the radius-to-thickness ratio on the fundamental frequency parameter of FG-CNTRC skewed cylindrical panels with simply supported and fully clamped boundary conditions are investigated in Fig. 9. It is seen that for all values of the radius-to-thickness ratio, the frequency parameter increases when increasing the skew angle. Also, for a constant value of the skew angle, the frequency parameter decreases by increasing the radius of the skewed panels and almost for the radius-to-thickness ratios larger than 100, the frequency parameter becomes insensitive to increase in the parameter R/h. This means that for $R/h > 100$ the curved skewed panels degenerate to skewed flat plates.

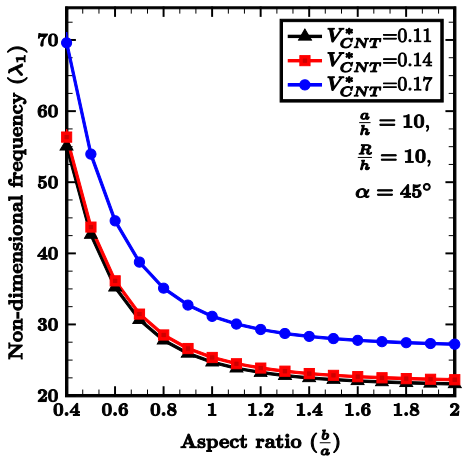

Fig. 11 Variation of the fundamental frequency parameter against the aspect ratio for the fully clamped FG-CNTRC skewed cylindrical panels with FG-X distribution of CNTs and different values of their volume fraction

Table 9 Non-dimensional frequency parameters ($\lambda_i = \omega_i a^2/h\sqrt{\rho_m/E_m}$) of the FG-CNTRC skewed cylindrical panels with different length-to-thickness ratio and CNTs distribution ($R/h = 10, \theta_0 = 60°, \alpha = 45°, V^*_{\mathrm{CNT}} = 0.17$)

	a/h	Method	UD				FG-X			
			λ_1	λ_2	λ_3	λ_4	λ_1	λ_2	λ_3	λ_4
C–C–C–C	10	TDQ	27.220	31.404	39.518	48.842	28.068	32.497	40.938	50.006
		ANSYS[a]	26.802	30.965	38.990	48.063	–	–	–	–
	20	TDQ	43.702	46.626	55.699	69.659	46.420	49.536	59.049	73.633
		ANSYS	43.260	46.168	55.215	69.093	–	–	–	–
S–S–S–S	10	TDQ	22.089	25.593	33.509	44.093	23.616	27.140	35.186	45.960
		ANSYS	21.329	24.505	32.140	42.358	–	–	–	–
	20	TDQ	32.224	33.932	42.368	56.755	34.878	36.820	45.620	60.654
		ANSYS	31.991	33.367	41.364	55.359	–	–	–	–
F–C–C–C	10	TDQ	23.204	26.800	31.317	39.385	23.979	27.658	32.445	40.806
		ANSYS	22.825	26.327	30.484	38.805	–	–	–	–
	20	TDQ	37.150	42.569	46.331	55.386	40.054	45.296	49.270	58.771
		ANSYS	36.803	41.977	45.820	54.836	–	–	–	–
C–S–C–S	10	TDQ	22.823	28.371	37.897	47.065	24.377	29.980	39.626	48.763
		ANSYS	22.037	27.290	36.519	44.591	–	–	–	–
	20	TDQ	32.504	36.697	48.517	64.916	35.209	39.718	51.993	69.106
		ANSYS	32.231	36.058	47.471	63.465	–	–	–	–
F–C–F–C	10	TDQ	23.162	23.227	26.518	31.116	23.925	24.011	27.393	32.272
		ANSYS	22.793	22.837	26.011	30.586	–	–	–	–
	20	TDQ	37.086	37.210	41.815	45.677	39.990	40.111	44.539	48.663
		ANSYS	36.724	36.880	41.170	45.006	–	–	–	–
F–S–F–S	10	TDQ	18.012	18.304	22.752	28.875	19.648	19.940	24.273	30.453
		ANSYS	17.359	17.560	21.497	27.149	–	–	–	–
	20	TDQ	23.384	23.724	30.411	36.503	26.651	26.945	33.267	39.675
		ANSYS	23.255	23.779	29.725	35.166	–	–	–	–

[a] Element type: SHELL181, number of element in each direction: 150

The effects of volume fraction on the fundamental frequency parameter of the FG-CNTRC skewed cylindrical panels with different boundary conditions and for two different values of the skew angle are investigated in Fig. 10. The results demonstrate that increasing the constraints at the edges of the panels leads to increase in the fundamental frequency parameter for all values of the CNT volume fraction.

Figure 11 shows the impact of the aspect ratio (b/a) on the fundamental frequency parameter of the fully clamped FG-CNTRC skewed cylindrical panels with FG-X distribution of CNTs and for different values of their volume fraction. It can be noted that the frequency parameter decreases as the aspect ratio of the panels increases for all values of the volume fraction.

The effects of boundary conditions together with the length-to-thickness ratio and skew angle on the first four non-dimensional frequency parameters of the FG-CNTRC skewed cylindrical panels are shown in Tables 9

Table 10 Non-dimensional frequency parameters ($\lambda_i = \omega_i a^2/h\sqrt{\rho_m/E_m}$) of the FG-CNTRC skewed cylindrical panels with different skew angles and CNTs distribution ($R/h = 10, \theta_0 = 60°, a/h = 0.1, V^*_{\mathrm{CNT}} = 0.17$)

	α °	UD				FG-X			
		λ_1	λ_2	λ_3	λ_4	λ_1	λ_2	λ_3	λ_4
C–C–C–C	20	24.790	28.110	39.087	44.328	25.529	29.102	40.537	45.370
	40	26.338	30.345	39.171	46.985	27.149	31.407	40.591	48.049
	60	34.012	37.685	43.336	50.391	35.096	38.941	44.801	52.048
S–S–S–S	20	20.511	22.080	32.114	42.991	21.866	23.487	33.794	44.465
	40	21.536	24.540	32.942	44.256	23.001	26.039	34.610	46.114
	60	25.836	30.286	36.880	44.744	27.751	32.113	38.716	46.685
F–C–C–C	20	21.450	23.238	28.347	33.456	22.131	23.936	29.344	33.867
	40	22.590	25.680	30.382	38.488	23.335	26.492	31.484	39.016
	60	27.311	34.002	37.523	42.922	28.266	35.102	38.806	44.410
C–S–C–S	20	21.096	25.443	37.473	43.360	22.489	26.925	39.220	44.835
	40	22.236	27.478	37.598	45.580	23.733	29.045	39.320	47.145
	60	26.508	32.353	40.145	48.576	28.425	34.203	42.023	50.535
F–C–F–C	20	21.354	21.424	22.988	26.579	22.043	22.090	23.741	26.780
	40	22.548	22.593	25.326	30.258	23.279	23.347	26.159	31.394
	60	27.299	27.323	33.993	37.374	28.251	28.281	35.107	38.681
F–S–F–S	20	16.908	16.992	19.484	26.542	18.428	18.483	20.887	26.774
	40	17.655	17.862	21.737	28.081	19.241	19.459	23.211	29.636
	60	20.238	20.574	27.347	32.995	22.140	22.430	29.186	34.807

and 10, respectively. Panels with both uniform and FG-X distributions of CNTs are analyzed. For the purpose of comparison, the panels with UD of CNTs are also analyzed using the commercial software ANSYS and the results are reported in Table 9. The element type "SHELL181" (150 elements in each x- and s-directions) is utilized to simulate the panels in this package. Good agreement between the results of the present approach and those of ANSYS software is observable. Also, it is seen that the frequency parameters considerably depend on the types of boundary conditions.

6 Conclusions

The free vibration behavior of FG-CNTRC skewed cylindrical panels under different types of boundary conditions was studied. The governing equations were derived based on the FSDT of shells. An extended version of the DQM, which is composed of the conventional DQM and geometrical transformation laws, was employed to discretize the strong form of the governing equations and the related boundary conditions. As a special case, the presented formulation can easily be degenerated to those of functionally graded skewed panels with ceramic and metal constituents. The fast rate of convergence and close agreements with the available results in the open literature and also those obtained by means of commercial software ANSYS demonstrate the accuracy, numerical stability and reliability features of the presented approach. The effects of various material and geometric parameters such as different distributions and volume fractions of CNTs, skew angle, length-to-thickness, radius-to-thickness and aspect ratios on the frequency parameters of the FG-CNTRC skewed cylindrical panels subjected to different boundary conditions are examined. The results showed that the skewed panels with FG-X and FG-O distributions of CNTs have the greatest and lowest natural frequencies. It was shown that the skew angle, radius-to-thickness ratio, aspect ratio and CNTs volume fraction considerably affect the frequency parameters. The data presented in this work can be used for a comprehensive study of the vibrational behavior of FG-CNTRC skewed cylindrical panels having different patterns of CNTs distributions and boundary conditions.

References

1. Ramaratnam, A.: Reinforcement of piezoelectric polymers with carbon nanotubes: pathway to next-generation sensors. J. Intell. Mater. Syst. Struct. **17**, 199–208 (2006)
2. Liew, K.M., Lei, Z.X., Zhang, L.W.: Mechanical analysis of functionally graded carbon nanotube reinforced composites: a review. Compos. Struct. **120**, 90–97 (2015)
3. Viet, N.V., Wang, Q., Kuo, W.S.: A studying on load transfer in carbon nanotube/epoxy composites under tension. J. Model. Mech. Mater. (2017). doi:10.1515/jmmm-2016-0153

4. Ruoff, R.S., Lorents, D.C.: Mechanical and thermal properties of carbon nanotubes. Carbon **33**, 925–930 (1995)
5. Lin, F., Xiang, Y.: Vibration of carbon nanotube reinforced composite beams based on the first and third order beam theories. Appl. Math. Model. **38**, 3741–3754 (2014)
6. Ansari, R., Faghih Shojaei, M., Mohammadi, V., Gholami, R., Sadeghi, F.: Nonlinear forced vibration analysis of functionally graded carbon nanotube-reinforced composite Timoshenko beams. Compos. Struct. **113**, 316–327 (2014)
7. Shen, H.-S.: Postbuckling of functionally graded fiber reinforced composite laminated cylindrical shells, part I: theory and solutions. Compos. Struct. **94**, 1305–1321 (2012)
8. Jam, J.E., Kiani, Y.: Low velocity impact response of functionally graded carbon nanotube reinforced composite beams in thermal environment. Compos. Struct. **132**, 35–43 (2015)
9. Ghorbani Shenas, A., Malekzadeh, P., Ziaee, S.: Vibration analysis of pre-twisted functionally graded carbon nanotube reinforced composite beams in thermal environment. Compos. Struct. **162**, 325–340 (2017)
10. Lei, Z.X., Zhang, L.W., Liew, K.M.: Analysis of laminated CNT reinforced functionally graded plates using the element-free kp-Ritz method. Compos. Part B Eng. **84**, 211–221 (2016)
11. Lei, Z.X., Zhang, L.W., Liew, K.M.: Free vibration analysis of laminated FG–CNT reinforced composite rectangular plates using the kp-Ritz method. Compos. Struct. **127**, 245–259 (2015)
12. Zhang, L.W.: An element-free based IMLS-Ritz method for buckling analysis of nanocomposite plates of polygonal planform. Eng. Anal. Bound. Elem. **77**, 10–25 (2017)
13. Setoodeh, A.R., Shojaee, M.: Critical buckling load optimization of functionally graded carbon nanotube-reinforced laminated composite quadrilateral plates. Polym. Compos. (2017). doi:10.1002/pc.24289
14. Zhang, L.W., Liew, K.M.: Element-free geometrically nonlinear analysis of quadrilateral functionally graded material plates with internal column supports. Compos. Struct. **147**, 99–110 (2016)
15. Zhang, L.W., Liew, K.M.: Postbuckling analysis of axially compressed CNT reinforced functionally graded composite plates resting on Pasternak foundations using an element-free approach. Compos. Struct. **138**, 40–51 (2016)
16. Zhang, L.W., Liew, K.M.: Geometrically nonlinear large deformation analysis of functionally graded carbon nanotube reinforced composite straight-sided quadrilateral plates. Comput. Methods Appl. Mech. Eng. **295**, 219–239 (2015)
17. Zhang, L.W., Liew, K.M., Jiang, Z.: An element-free analysis of CNT-reinforced composite plates with column supports and elastically restrained edges under large deformation. Compos. Part B Eng. **95**, 18–28 (2016)
18. Zhang, L.W.: Geometrically nonlinear large deformation of CNT-reinforced composite plates with internal column supports. J. Model. Mech. Mater. (2017). doi:10.1515/jmmm-2016-0154
19. Zhang, L.W., Liew, K.M., Reddy, J.N.: Postbuckling behavior of bi-axially compressed arbitrarily straight-sided quadrilateral functionally graded material plates. Comput. Methods Appl. Mech. Eng. **300**, 593–610 (2016)
20. Zhang, L.W., Liew, K.M., Reddy, J.N.: Postbuckling analysis of bi-axially compressed laminated nanocomposite plates using the first-order shear deformation theory. Compos. Struct. **152**, 418–431 (2016)
21. Zhang, L.W., Liew, K.M., Reddy, J.N.: Postbuckling of carbon nanotube reinforced functionally graded plates with edges elastically restrained against translation and rotation under axial compression. Comput. Methods Appl. Mech. Eng. **298**, 1–28 (2016)
22. Lei, Z.X., Zhang, L.W., Liew, K.M.: Elastodynamic analysis of carbon nanotube-reinforced functionally graded plates. Int. J. Mech. Sci. **99**, 208–217 (2015)
23. Zhang, L.W., Song, Z.G., Liew, K.M.: Optimal shape control of CNT reinforced functionally graded composite plates using piezoelectric patches. Compos. Part B Eng. **85**, 140–149 (2016)
24. Zhang, L.W., Song, Z.G., Liew, K.M.: Nonlinear bending analysis of FG–CNT reinforced composite thick plates resting on Pasternak foundations using the element-free IMLS-Ritz method. Compos. Struct. **128**, 165–175 (2015)
25. Zhang, L.W., Song, Z.G., Liew, K.M.: State-space Levy method for vibration analysis of FG–CNT composite plates subjected to in-plane loads based on higher-order shear deformation theory. Compos. Struct. **134**, 989–1003 (2015)
26. Malekzadeh, P., Shojaee, M.: Buckling analysis of quadrilateral laminated plates with carbon nanotubes reinforced composite layers. Thin Walled Struct. **71**, 108–118 (2013)
27. Zhang, L.W., Xiao, L.N., Zou, G.L., Liew, K.M.: Elastodynamic analysis of quadrilateral CNT-reinforced functionally graded composite plates using FSDT element-free method. Compos. Struct. **148**, 144–154 (2016)
28. Zhang, L.W., Zhang, Y., Zou, G.L., Liew, K.M.: Free vibration analysis of triangular CNT-reinforced composite plates subjected to in-plane stresses using FSDT element-free method. Compos. Struct. **149**, 247–260 (2016)
29. Zhang, L.W., Zhu, P., Liew, K.M.: Thermal buckling of functionally graded plates using a local Kriging meshless method. Compos. Struct. **108**, 472–492 (2014)
30. Zhu, P., Zhang, L.W., Liew, K.M.: Geometrically nonlinear thermomechanical analysis of moderately thick functionally graded plates using a local Petrov–Galerkin approach with moving Kriging interpolation. Compos. Struct. **107**, 298–314 (2014)
31. Fantuzzi, N., Tornabene, F., Bacciocchi, M., Dimitri, R.: Free vibration analysis of arbitrarily shaped functionally graded carbon nanotube-reinforced plates. Compos. Part B Eng. (2016). doi:10.1016/j.compositesb.2016.09.021
32. Shen, H.-S.: Nonlinear bending of functionally graded carbon nanotube-reinforced composite plates in thermal environments. Compos. Struct. **91**, 9–19 (2009)
33. Lei, Z.X., Liew, K.M., Yu, J.L.: Free vibration analysis of functionally graded carbon nanotube-reinforced composite plates using the element-free kp-Ritz method in thermal environment. Compos. Struct. **106**, 128–138 (2013)
34. Abdollahzadeh Shahrbabaki, E., Alibeigloo, A.: Three-dimensional free vibration of carbon nanotube-reinforced composite plates with various boundary conditions using Ritz method. Compos. Struct. **111**, 362–370 (2014)
35. Malekzadeh, P., Zarei, A.R.: Free vibration of quadrilateral laminated plates with carbon nanotube reinforced composite layers. Thin Walled Struct. **82**, 221–232 (2014)
36. Malekzadeh, P., Heydarpour, Y.: Mixed Navier-layerwise differential quadrature three-dimensional static and free vibration analysis of functionally graded carbon nanotube reinforced composite laminated plates. Meccanica **50**, 143–167 (2015)
37. Wattanasakulpong, N., Chaikittiratana, A.: Exact solutions for static and dynamic analyses of carbon nanotube-reinforced composite plates with Pasternak elastic foundation. Appl. Math. Model. **39**, 5459–5472 (2015)

38. Malekzadeh, P., Dehbozorgi, M., Monajjemzadeh, S.M.: Vibration of functionally graded carbon nanotube-reinforced composite plates under a moving load. Sci. Eng. Compos. Mater. **22** (2015). doi:10.1515/secm-2013-0142
39. Zhang, L.W., Cui, W.C., Liew, K.M.: Vibration analysis of functionally graded carbon nanotube reinforced composite thick plates with elastically restrained edges. Int. J. Mech. Sci. **103**, 9–21 (2015)
40. Zhang, L.W., Lei, Z.X., Liew, K.M.: Computation of vibration solution for functionally graded carbon nanotube-reinforced composite thick plates resting on elastic foundations using the element-free IMLS-Ritz method. Appl. Math. Comput. **256**, 488–504 (2015)
41. Wu, C.-P., Li, H.-Y.: Three-dimensional free vibration analysis of functionally graded carbon nanotube-reinforced composite plates with various boundary conditions. J. Vib. Control **22**, 89–107 (2016)
42. Kiani, Y.: Free vibration of FG–CNT reinforced composite skew plates. Aerosp. Sci. Technol. **58**, 178–188 (2016)
43. Malekzadeh, P., Dehbozorgi, M.: Low velocity impact analysis of functionally graded carbon nanotubes reinforced composite skew plates. Compos. Struct. **140**, 728–748 (2016)
44. García-Macías, E., Castro-Triguero, R., Saavedra Flores, E.I., Friswell, M.I., Gallego, R.: Static and free vibration analysis of functionally graded carbon nanotube reinforced skew plates. Compos. Struct. **140**, 473–490 (2016)
45. Ansari, R., Shahabodini, A., Faghih Shojaei, M.: Vibrational analysis of carbon nanotube-reinforced composite quadrilateral plates subjected to thermal environments using a weak formulation of elasticity. Compos. Struct. **139**, 167–187 (2016)
46. Setoodeh, A.R., Shojaee, M.: Application of TW–DQ method to nonlinear free vibration analysis of FG carbon nanotube-reinforced composite quadrilateral plates. Thin Walled Struct. **108**, 1–11 (2016)
47. Zhang, L.W., Lei, Z.X., Liew, K.M.: Buckling analysis of FG–CNT reinforced composite thick skew plates using an element-free approach. Compos. Part B Eng. **75**, 36–46 (2015)
48. Zhang, L.W.: On the study of the effect of in-plane forces on the frequency parameters of CNT-reinforced composite skew plates. Compos. Struct. **160**, 824–837 (2017)
49. Zhang, L.W., Liu, W.H., Liew, K.M.: Geometrically nonlinear large deformation analysis of triangular CNT-reinforced composite plates. Int. J. Nonlinear Mech. **86**, 122–132 (2016)
50. Zhang, L.W., Liew, K.M.: Large deflection analysis of FG–CNT reinforced composite skew plates resting on Pasternak foundations using an element-free approach. Compos. Struct. **132**, 974–983 (2015)
51. Lei, Z.X., Zhang, L.W., Liew, K.M., Yu, J.L.: Dynamic stability analysis of carbon nanotube-reinforced functionally graded cylindrical panels using the element-free kp-Ritz method. Compos. Struct. **113**, 328–338 (2014)
52. Zhang, L.W., Song, Z.G., Liew, K.M.: Computation of aerothermoelastic properties and active flutter control of CNT reinforced functionally graded composite panels in supersonic airflow. Comput. Methods Appl. Mech. Eng. **300**, 427–441 (2016)
53. Zhang, L.W., Song, Z.G., Qiao, P., Liew, K.M.: Modeling of dynamic responses of CNT-reinforced composite cylindrical shells under impact loads. Comput. Methods Appl. Mech. Eng. **313**, 889–903 (2017)
54. Heydarpour, Y., Aghdam, M.M., Malekzadeh, P.: Free vibration analysis of rotating functionally graded carbon nanotube-reinforced composite truncated conical shells. Compos. Struct. **117**, 187–200 (2014)
55. Ansari, R., Torabi, J.: Numerical study on the buckling and vibration of functionally graded carbon nanotube-reinforced composite conical shells under axial loading. Compos. Part B Eng. **95**, 196–208 (2016)
56. Song, Z.G., Zhang, L.W., Liew, K.M.: Vibration analysis of CNT-reinforced functionally graded composite cylindrical shells in thermal environments. Int. J. Mech. Sci. **115–116**, 339–347 (2016)
57. Ansari, R., Torabi, J., Shojaei, M.F.: Vibrational analysis of functionally graded carbon nanotube-reinforced composite spherical shells resting on elastic foundation using the variational differential quadrature method. Eur. J. Mech. A Solids **60**, 166–182 (2016)
58. Kamarian, S., Salim, M., Dimitri, R., Tornabene, F.: Free vibration analysis of conical shells reinforced with agglomerated carbon nanotubes. Int. J. Mech. Sci. **108–109**, 157–165 (2016)
59. Sobhani Aragh, B., Nasrollah Barati, A.H., Hedayati, H.: Eshelby–Mori–Tanaka approach for vibrational behavior of continuously graded carbon nanotube-reinforced cylindrical panels. Compos. Part B Eng. **43**, 1943–1954 (2012)
60. Shen, H.-S., Xiang, Y.: Nonlinear vibration of nanotube-reinforced composite cylindrical shells in thermal environments. Comput. Methods Appl. Mech. Eng. **213–216**, 196–205 (2012)
61. Yas, M.H., Pourasghar, A., Kamarian, S., Heshmati, M.: Three-dimensional free vibration analysis of functionally graded nanocomposite cylindrical panels reinforced by carbon nanotube. Mater. Des. **49**, 583–590 (2013)
62. Pourasghar, A., Kamarian, S.: Three-dimensional solution for the vibration analysis of functionally graded multiwalled carbon nanotubes/phenolic nanocomposite cylindrical panels on elastic foundation. Polym. Compos. **34**, 2040–2048 (2013)
63. Shen, H.-S., Xiang, Y.: Nonlinear vibration of nanotube-reinforced composite cylindrical panels resting on elastic foundations in thermal environments. Compos. Struct. **111**, 291–300 (2014)
64. Zhang, L.W., Lei, Z.X., Liew, K.M., Yu, J.L.: Static and dynamic of carbon nanotube reinforced functionally graded cylindrical panels. Compos. Struct. **111**, 205–212 (2014)
65. Lei, Z.X., Zhang, L.W., Liew, K.M.: Vibration analysis of CNT-reinforced functionally graded rotating cylindrical panels using the element-free kp-Ritz method. Compos. Part B Eng. **77**, 291–303 (2015)
66. Lei, Z.X., Zhang, L.W., Liew, K.M.: Parametric analysis of frequency of rotating laminated CNT reinforced functionally graded cylindrical panels. Compos. Part B Eng. **90**, 251–266 (2016)
67. Mirzaei, M., Kiani, Y.: Free vibration of functionally graded carbon nanotube reinforced composite cylindrical panels. Compos. Struct. **142**, 45–56 (2016)
68. Jooybar, N., Malekzadeh, P., Fiouz, A.R.: Vibration of functionally graded carbon nanotubes reinforced composite truncated conical panels with elastically restrained against rotation edges in thermal environment. Compos. Part B Eng. **106**, 242–261 (2016)
69. Tornabene, F., Fantuzzi, N., Bacciocchi, M., Viola, E.: Effect of agglomeration on the natural frequencies of functionally graded carbon nanotube-reinforced laminated composite doubly-curved shells. Compos. Part B Eng. **89**, 187–218 (2016)
70. Thomas, B., Roy, T.: Vibration analysis of functionally graded carbon nanotube-reinforced composite shell structures. Acta Mech. **227**, 581–599 (2016)

71. Pouresmaeeli, S., Fazelzadeh, S.A.: Frequency analysis of doubly curved functionally graded carbon nanotube-reinforced composite panels. Acta Mech. (2016). doi:10.1007/s00707-016-1647-9
72. Tornabene, F., Fantuzzi, N., Bacciocchi, M.: Linear static response of nanocomposite plates and shells reinforced by agglomerated carbon nanotubes. Compos. Part B Eng. (2016). doi:10.1016/j.compositesb.2016.07.011
73. Reddy, J.N.: Theory and Analysis of Elastic Plates and Shells, 2nd edn. CRC Press, Hoboken (2006)
74. Reddy, J.N.: Mechanics of Laminated Composite Plates and Shells: Theory and Analysis. CRC Press, Boca Raton (2004)
75. Berthelot, J.-M.: Composite Materials: Mechanical Behavior and Structural Analysis. Springer, New York (1999)
76. Zhang, L.W., Huang, D., Liew, K.M.: An element-free IMLS-Ritz method for numerical solution of three-dimensional wave equations. Comput. Methods Appl. Mech. Eng. **297**, 116–139 (2015)
77. Zhang, L.W., Li, D.M., Liew, K.M.: An element-free computational framework for elastodynamic problems based on the IMLS-Ritz method. Eng. Anal. Bound. Elem. **54**, 39–46 (2015)
78. Tornabene, F., Fantuzzi, N., Bacciocchi, M.: The strong formulation finite element method: stability and accuracy. Fract. Struct. Integr. **29**, 251–265 (2014)
79. Tornabene, F., Fantuzzi, N., Ubertini, F., Viola, E.: Strong formulation finite element method based on differential quadrature: a survey. Appl. Mech. Rev. **67**, 020801–020856 (2015)
80. Malekzadeh, P., Shojaee, M.: A two-variable first-order shear deformation theory coupled with surface and nonlocal effects for free vibration of nanoplates. J. Vib. Control **21**, 2755–2772 (2015)
81. Malekzadeh, P., Shojaee, M.: Free vibration of nanoplates based on a nonlocal two-variable refined plate theory. Compos. Struct. **95**, 443–452 (2013)
82. Malekzadeh, P., Golbahar Haghighi, M.R., Shojaee, M.: Nonlinear free vibration of skew nanoplates with surface and small scale effects. Thin Walled Struct. **78**, 48–56 (2014)
83. Han, Y., Elliott, J.: Molecular dynamics simulations of the elastic properties of polymer/carbon nanotube composites. Comput. Mater. Sci. **39**, 315–323 (2007)
84. Kandasamy, S., Singh, A.V.: Free vibration analysis of skewed open circular cylindrical shells. J. Sound Vib. **290**, 1100–1118 (2006)